Received: 22 December 2022 | Revised: 22 June 2023 | Accepted: 10 July 2023

DOI: 10.1002/qj.4523

Quarterly Journal of the Royal Meteorological Society RMetS

RESEARCH ARTICLE

Horizontal kinetic energy analysis of tropical transition simulations with the WRF and HARMONIE-AROME models

Carlos Calvo-Sancho[1] | **Pedro Bolgiani**[2] | **Álvaro Subias**[3] | **Mariano Sastre**[2] | **Juan Jesús González-Alemán**[3] | **María Luisa Martín**[1,4]

[1]Department of Applied Mathematics, Faculty of Computer Engineering, Universidad de Valladolid, Segovia, Spain

[2]Department of Earth Physics and Astrophysics, Faculty of Physics, Universidad Complutense de Madrid, Madrid, Spain

[3]Agencia Estatal de Meteorología (AEMET), Madrid, Spain

[4]Interdisciplinary Mathematics Institute, Universidad Complutense de Madrid, Madrid, Spain

Correspondence
Carlos Calvo-Sancho, Department of Applied Mathematics. Faculty of Computer Engineering, Universidad de Valladolid, Segovia, Spain.
Email: carlos.calvo.sancho@uva.es

Funding information
European Centre for Medium-Range Weather Forecasts; Ministerio de Ciencia e Innovación, Grant/Award Numbers: PID2019-105306RB-I00, PRE2020-092343; Interdisciplinary Mathematics Institute of the Complutense University of Madrid

Abstract

Four tropical transition (TT) events in the North Atlantic basin are simulated with the Weather Research and Forecasting (WRF) and the HARMONIE-AROME (HAR) models to study the main features of the horizontal kinetic energy (HKE) spectra of these kinds of high-energetic atmospheric system. Though most of the times similar results are obtained with both models, HAR shows a more intense filtering and numerical dissipation, whereas WRF tends to represent overenergized spectra in the synoptic scale and especially at smaller wavelengths. Predictability is dissimilar for the four TTs studied due to the different spectral curve slope obtained for each case, ranging from unlimited to very poor predictability at synoptic scale. Additionally, an increased HKE is presented in the middle–upper troposphere spectra. A deep analysis of the different terms involved in the equation of the spectral energy budget is presented through a detailed study of one of these TTs. The role of all of them is studied, connecting the energy spectra and the meteorological processes involved. The energy budget terms related to the nonlinear spectral transfer, the three-dimensional divergence, and diabatic process tendencies are identified as the key ones, whereas the potential and kinetic conversion terms and the vertical flux HKE and pressure divergence terms play a secondary role on modulating the spectrum behaviour. The major energetic contributions are found at the synoptic scale, but results show that a two-dimensional energy cascade does not fully capture the whole spectrum of a TT. The role of convection, latent heat release, and moist convection outbursts is sketched and a link within different vertical levels is found. Results show that a high-energetic system, such as a TT, can effectively alter the atmospheric energy behaviour.

KEYWORDS

energy spectrum, HARMONIE-AROME, horizontal kinetic energy, spectral energy budget, WRF

1 | INTRODUCTION

Tropical cyclones are fully barotropic, diabatic, warm-core cyclones. They have a barotropic origin in most of the cases; for example, they develop from easterly waves, tropical lows, or tropical troughs (McTaggart-Cowan *et al.*, 2013). On the other hand, under the appropriate baroclinic atmospheric environments, a series of precursor disturbances may develop a tropical cyclogenesis (Gray, 1968; DeMaria *et al.*, 2001; McTaggart-Cowan *et al.*, 2013). One of the possible disturbances can be a tropical transition (TT). The TT is a form of tropical cyclogenesis associated with extratropical precursors in which a baroclinic cyclone evolves and mutates into a tropical cyclone when affected by an upper tropospheric disturbance originating in midlatitudes (Davis and Bosart, 2003, 2004; Hulme and Martin, 2009; Galarneau *et al.*, 2015; McTaggart-Cowan *et al.*, 2015; Bentley *et al.*, 2017; Calvo-Sancho *et al.*, 2022). The upper tropospheric disturbance is frequently formed in conjunction with breaking Rossby waves (McIntyre and Palmer, 1983; Thorncroft *et al.*, 1993; Martius *et al.*, 2008), which can arise in an assortment of phenomena: cut-off lows (Palmén and Newton, 1969; Nieto *et al.*, 2005), potential vorticity streamers (Martius *et al.*, 2008; Galarneau *et al.*, 2015), and tropical upper tropospheric trough cells (Sadler, 1976; Ferreira and Schubert, 1999; Patla *et al.*, 2009). Upper tropospheric disturbances have the potential to develop TTs in environments characterized by low sea-surface temperature (McTaggart-Cowan *et al.*, 2015; Calvo-Sancho *et al.*, 2022) and moderate-to-high vertical wind shear (Bracken and Bosart, 2000; Molinari *et al.*, 2004; McTaggart-Cowan *et al.*, 2008, 2013; Calvo-Sancho *et al.*, 2022). Therefore, a TT is the process whereby a baroclinic extratropical or subtropical cyclone, commonly presenting high-to-moderate vertical wind shear, is transformed into a warm-core, low vertical wind shear tropical cyclone. In other words, during a TT the cold-core cyclone progressively loses its asymmetrical nature and acquires the typical features of warm-core symmetrical tropical cyclones.

Tropical cyclones formed via TTs are likely to affect Europe, since they occur in the Subtropics and midlatitudes. In fact, western Europe has been recently threatened by several cyclones with this type of genesis. Hurricanes such as *Ophelia* (2017) or *Vince* (2005) almost reached the Iberian Peninsula, whereas *Leslie* (2018) directly affected its northern area (Tapiador *et al.*, 2007; Beven *et al.*, 2008). Furthermore, extratropical transition of ex-Hurricane *Ophelia* severely affected Ireland (Moore, 2021). Calvo-Sancho *et al.* (2022) analysed 30 TT events over the central and eastern North Atlantic basin during the period 1979–2019, studying their synoptic environments to highlight their common features and differences. In this study, the importance of potential vorticity redistribution and latent heat release on the transition time is emphasized. In fact, the transition time is accompanied by a large latent heat release that promotes the vertical redistribution of potential vorticity and a reduction of the 850–300 hPa vertical wind shear. Differences between the analysed TTs developed in the central and the eastern North Atlantic are shown. Though the TT environments in the central North Atlantic predominantly show warm sea-surface temperatures (>25°C) and low-to-moderate wind shear (<15 $m \cdot s^{-1}$), the eastern North Atlantic ones develop in low sea-surface temperature values (<25°C) and high wind shear (>15 $m \cdot s^{-1}$). Tropical cyclones have a severe impact on population safety, ecological systems, and the economy, producing widespread hazards and damage. The most common include large effects on infrastructures, agriculture, tourism, and even human losses (Peduzzi *et al.*, 2012; Lenzen *et al.*, 2019). Consequently, improving the understanding of these events would yield an essential socio-economic benefit, particularly for the Iberian and western Europe regions (Galarneau *et al.*, 2015).

The assessment of the energy spectrum is fundamental in many studies to depict the basic atmospheric status of the system (Bierdel *et al.*, 2012). The spectrum analysis reveals the energy distribution across different scales for a particular atmospheric situation, and how this distribution changes as the energy is transferred between scales as a function of the wave numbers (Peng *et al.*, 2014a; Sun *et al.*, 2017). Furthermore, an energetic budget assessment presents the total tendency of the atmospheric energy. This will show the exchange of energy between different atmospheric levels and the conversions between kinetic, potential, or thermodynamic forms. For these reasons, the energy spectrum and the energetic budget analysis appear as especially appropriate to characterize the genesis and evolution of complex systems like the TTs. The scientific literature about the subject shows that different variables can be considered to obtain the atmospheric energy spectra. Nastrom and Gage (1985) use potential temperature in their study, and Cho *et al.* (1999) derive the energy spectra from trace gases; however, horizontal kinetic energy (HKE) derived from wind speed is the variable used most because of its simplicity and the availability of observations (Nastrom and Gage, 1985; Skamarock, 2004; Bolgiani *et al.*, 2022).

The atmospheric HKE spectrum has been largely discussed in the scientific literature. The current knowledge agrees on the fact that synoptic scale phenomena (here defined as wavelengths $\lambda_h > 400$ km) follow a horizontal wave-number spectral curve proportional to k^{-3} (Kolmogorov, 1941), whereas at mesoscale wavelengths

($400 > \lambda_h > 4$ km) the atmospheric energy is known to dissipate proportionally to $k^{-5/3}$ (Nastrom and Gage, 1985; Lindborg, 1999). These are just approximations to the actual curve, which is estimated to be much more complex (Lindborg, 1999); however, it is generally agreed that the transition between these two power-law dependences takes place at $\lambda_h \approx 500$ km (Cho *et al.*, 1999; Lindborg, 1999). These differences between the power-law k^{-3} and $k^{-5/3}$ dependences of the atmospheric energy are crucial to understand the role of the different scales. Although the formation mechanisms of the energetic curve are still a topic of research, particularly for the mesoscale $k^{-5/3}$ slope (Gage, 1979; Tung and Orlando, 2003; Skamarock, 2004; Tulloch and Smith, 2006; Wang *et al.*, 2018; Zheng *et al.*, 2020), the observed atmospheric spectrum has been replicated by many numerical weather prediction (NWP) models (Skamarock, 2004; Hamilton *et al.*, 2008; Skamarock *et al.*, 2014). Understanding the dynamics of the mesoscale HKE spectrum provides knowledge beyond the academic interest and into practical terms, as it is crucial to computing error growth and numerical forecasting system accuracy (Lorenz, 1969; Ricard *et al.*, 2013; Skamarock *et al.*, 2014; Weyn and Durran 2017). In fact, the energy spectrum analysis is an important tool to evaluate the model's ability in resolving atmospheric features at various scales and to assess the effective resolution (Skamarock, 2004; Abdalla *et al.*, 2013), when compared against available theoretical power-law dependence spectra (Lindborg, 1999). In addition, Lorenz (1969) concluded that the upscale transmission over time of small-scale error provides an effective limit to the predictability of flows. Thus, for an atmospheric flow spectrum governed by a k^{-p} power-law behaviour, the error-doubling time decreases with scale when $p < 3$; this fast doubling of the upstream errors renders the flow into a chaotic system, which is inherently limited in its mathematical predictability. This has already been verified by several studies using full-physics simulations (Selz and Craig 2015; Sun and Zhang, 2016; Sun *et al.*, 2017). Also, according to Lorenz (1969), there is no such limit for flows with $p \geq 3$ as the error-doubling times do not decrease with scale.

Recently, the contributions of different physical processes at various scales to the energy budget of the atmosphere have been under research using some modifications in the governing equations of NWP models (Koshyk and Hamilton, 2001; Waite and Snyder, 2013; Peng *et al.*, 2014a, 2014b; Peng *et al.*, 2015a; 2015b; Sun *et al.*, 2017; Wang *et al.*, 2018; Zheng *et al.*, 2020). Peng *et al.* (2014b) analyse the role of the latent heat flux and deep convection on the spectral kinetic energy budget of the Mei-yu frontal system, highlighting the contribution of latent heat in the increasing of the kinetic energy in upper levels. They assert that the kinetic energy in the upper troposphere is deposited via buoyancy flux; that is, conversion of available potential energy (APE) to HKE, whereas in the lower troposphere the mesoscale kinetic energy is deposited through nonlinear advective terms and vertical pressure flux divergence. In the mature phase of the frontal system, the mesoscale kinetic energy spectrum follows a horizontal wave-number spectral curve proportional to $k^{-5/3}$ for the smaller scales, presenting a buoyancy term that suggests a significant input of kinetic energy in mesoscale. Sun *et al.* (2017) use a high-resolution cloud model ensemble to simulate organized convective systems under vertical wind shear and study the associated kinetic energy spectrum. They find that the convective systems can generate by themselves a background mesoscale kinetic energy spectrum following a curve proportional to $k^{-5/3}$. Sensitivity experiments doubling the domain size show robust results in terms of different model settings, proving a similar spectrum and showing that the curve is not affected by the organization of the convective systems. Using high-resolution simulations, Wang *et al.* (2018) study the HKE spectra of an idealized tropical cyclone at several atmospheric levels during its intensification and mature stages. They find a spectrum with a higher than expected spectral curve slope at the mesoscale, resembling a hump in the curve, both for the lower and upper troposphere, in discrepancy with previous observations (Lindborg, 1999). Additionally, their vertically averaged spectral budget distribution as a function of wave numbers shows the specific roles of different physical processes (convection, buoyancy, vertical propagation of inertia–gravity waves). In line with these results, Zheng *et al.* (2020) analyse mesoscale model simulations of a particular case study from the Pacific Ocean basin, concluding that a tropical cyclone can alter the canonical atmospheric energy spectrum during its evolution.

The present study is part of the IBERCANES research project on TT analysis and simulations with different NWP models. Before evaluating the meteorological characteristics of these simulations, possible limitations must be assessed, as we are dealing with high-resolution simulations, verging on the design limits of the models. Thus, the first step was to generate a seasonal climatology of the HKE spectra (Bolgiani *et al.*, 2022), both for the Northern Hemisphere (periodic domain) and for the North Atlantic area (limited-area domain) using the fifth generation of the European Centre for Medium-Range Weather Forecasts (ECMWF) Atmospheric Reanalysis (ERA5; Hersbach *et al.*, 2020). The results exhibit that ERA5 is properly capturing the synoptic conditions with remarkable differences between the latitudinal domains. However, the reanalysis's spectra are not able to properly reproduce the spectral curve slope rates at mesoscale due to the ERA5 horizontal resolution, which is a source of uncertainties

to be considered when using this dataset. The seasonal variability emphasizes different energetic features throughout seasons, with winter being the most energetic season and summer the least. The limited-area North Atlantic domain results produce larger energy densities and ranges.

Since the skill to reproduce the theoretical power-law dependence spectra is regularly shown as evidence of the accuracy of the formulation, implementation, and configuration of an atmospheric model (Skamarock *et al.*, 2014), in the current study the HKE spectra for several high-energetic atmospheric systems, such as TTs, is evaluated using two NWP models. The most severe TTs analysed by Calvo-Sancho *et al.* (2022) are selected and simulated using two NWP models: the mesoscale Weather Research and Forecasting (WRF) and the HARMONIE-AROME. The ERA5 climatology of the HKE spectra is used as a reference curve to compare against in this study, highlighting the value of high-resolution simulations in the spectrum results and how the models assume and manage the atmospheric energy in the simulation. The HKE spectra of the TT simulations are compared to evaluate the energetic behaviour of these particular events and possible differences between the NWP models. Also, one of the TTs is selected to assess the spectral budget and the development and transmission of the energy cascade (Lindborg, 1999); that is, the energy transfer from large to small scales of motion (direct energy cascade) or from small to large scales (inverse energy cascade) during the event. The final purpose of this study is to evaluate the ability of the models in properly simulating and diagnosing TTs, as only scarce literature exists on this topic and is almost non-existent for the HARMONIE-AROME model. This is expected to be supportive for the interpretation of other studies that include a large set of TT simulations (Calvo-Sancho *et al.*, 2022).

This work is organized as follows: Section 2 presents the data used and methodology followed to obtain the results, which are shown and discussed in Section 3. Section 4 yields the conclusions of this study.

2 | DATA AND METHODOLOGY

2.1 | Experimental set-up

Calvo-Sancho *et al.* (2022) used the Hurricane Database 2 (Landsea and Franklin, 2013) to compute the wind-speed percentile of whole TTs occurring over the North Atlantic, which encompasses 060°W–000°W of longitude and 20°N–90°N of latitude. Over this dataset, percentiles of wind speed are derived. The TTs analysed here are selected considering those equal or above the 90th percentile for wind-speed values (Table 1). These selected events are then simulated by employing two high-resolution limited-area NWP models: the already settled and highly approved Advanced Research WRF model, version 4.0.3 (Skamarock *et al.*, 2008), and the operational HARMONIE-AROME model, cycle 43 h2.21 (HAR hereafter; Bengtsson *et al.*, 2017). The simulations with both models are allowed a 6 hr spin-up, covering from 42 hr before to 30 hr after the TT evaluated, with a 3 hr output.

The non-hydrostatic WRF model is configured with two domains under a two-way nesting strategy. Each domain is 1,000 × 1,000 grid points, with a horizontal resolution of 7.5 km for the outer domain (D01) and 2.5 km for the inner domain (D02). The vertical resolution is 65 sigma levels unequally spaced, with a greater resolution in the lower troposphere to obtain a better representation of the convective processes in the planetary boundary layer. The WRF model allows for a flexible computing mode, called adaptative time step, enabling the modulation of time steps used in the simulation for increasing the model efficiency (Hutchinson, 2007); therefore, the calculations are not performed at fixed time steps but vary within a short range. Adaptative time steps are used here with the default WRF hurricane research configuration.

TABLE 1 Selection of TTs above the 90th percentile wind-speed values during the period 1979–2020.

NHC code	Storm name	Transition time	Latitude (°N)	Longitude (°W)	Sea-level pressure (hPa)	Maximum sustained wind speed ($m \cdot s^{-1}$)
AL292005	*Delta*	1200 UTC November 23, 2005	27.4	041.2	989	25.7
AL172017	*Ophelia*	0600 UTC October 9, 2017	30.9	040.0	1,012	18.0
AL132018	*Leslie*	1800 UTC September 29, 2018	34.3	051.3	994	23.1
AL302020	*Theta*	1800 UTC November 10, 2020	29.0	036.7	987	30.9

Note: Latitude, longitude, and sea-level pressure are referred to the centre of minimum pressure of the storm. Note that the four systems transitioned into tropical cyclones. NHC: National Hurricane Center.

The most important physics parametrizations used are the WRF single-moment six-class scheme for microphysics (Hong and Lim, 2006), the Yonsei University scheme for the planetary boundary layer (Hong *et al.*, 2006), the Dudhia short-wave scheme (Dudhia, 1989) and the rapid radiative transfer model long-wave scheme (Mlawer *et al.*, 1997) for radiation. Cumulus is explicitly computed by the model in D02, whereas in D01 it is parameterized using the new Tiedtke scheme (Zhang and Wang, 2017). Finally, the initial/boundary conditions are obtained from ERA5 (Hersbach *et al.*, 2020) produced by the ECMWF with a 0.25° horizontal resolution and 6 hr temporal resolution.

To maintain the consistency of the study, the HAR model is configured to the resemblance of the WRF's set-up as far as possible, in accordance with previous studies comparing these two models for other meteorological phenomena (Román-Cascón *et al.*, 2019; Quitián-Hernández *et al.*, 2021; Díaz-Fernández, Bolgiani, Santos-Muñoz *et al.*, 2022; Díaz-Fernández, Bolgiani, Sastre *et al.*, 2022). A single domain with the same grid and horizontal resolution used for WRF D02 is defined. The vertical resolution, different to the WRF model, is 65 hybrid sigma-pressure vertical levels, and the HAR default physics options are used (Bengtsson *et al.*, 2017). The HAR model shares several of the physical parametrizations and the dynamical core used in the AROME model (Seity *et al.*, 2011). Both models share the Surface Externalisée surface parameterization scheme, the Morcrette short-wave radiation scheme (Seity *et al.*, 2011; Bengtsson *et al.*, 2017), and most of the ICE-3 microphysics package (Lascaux *et al.*, 2006). The HAR model employs the EDMFm scheme for shallow convection (de Rooy *et al.*, 2013; Bengtsson *et al.*, 2017) and the HARATU scheme (Bengtsson *et al.*, 2017) is used for parameterized turbulence. The temporal resolution is set at 30 s. The configuration is convection permitting by default, along with a non-hydrostatic spectral dynamical core using a semi-Lagrangian and semi-implicit discretization of the equations. This discretization allows one to resolve the mesoscale processes better, enabling more realistic results compared with other models (Bengtsson *et al.*, 2017), which may provide an added value to the study of TTs.

The initial/boundary conditions are the same as those used for WRF. It is also important to note that both models are energy dissipative; that is, both models filter out energy of the atmosphere at some point to maintain the physical variables under realistic conditions in the limited-area domain. This is done by the WRF and HAR models using numerical filters at low wavelengths, as initial/boundary conditions provide energy mostly at large wavelengths and a direct energy cascade is assumed (Kolmogorov, 1941; Lindborg, 1999).

2.2 | HKE methodology

2.2.1 | Spectra

The energy spectrum of each simulation is computed following the basic methodology set by Skamarock (2004) and the more specific methodology already applied in previous studies by Bolgiani *et al.* (2022). First, the wind-speed field is derived using the horizontal components u and v. Then, the average wind speed is removed to obtain the wind anomalies, which are detrended, rendering the non-periodic data from the limited-area simulation to periodic data, adequate for the spectral decomposition. A longitudinal-wise HKE spectral decomposition is performed using a one-dimensional discrete Fourier transform (Skamarock, 2004) and then averaged over latitude, generating a single result for each vertical level and time step. To account for energy-mass differences, the results are scaled by the average density of each level (Peng *et al.*, 2015a; Sun *et al.*, 2017). The results are presented in the commonly used energy density and wave-number plots. To ease the evaluation, temporal averages are shown in the results.

2.2.2 | Spectral budget

The spectral budget is analysed to increase the insight into the HKE dynamics, presenting the roles of the different physical processes in charge of the energy development and transfer. To allow for a proper comparison with the related literature, the budget computation follows a different methodology from the previous spectral analysis. The HKE is initially derived using the two-dimensional discrete cosine transform (DCT; Denis *et al.*, 2002). Let $\widehat{\varphi}(\mathbf{k})$ be the DCT of the field $\varphi(x,y)$, where $k_{\mathrm{h}} = |\mathbf{k}| = \left(k_x, k_y\right)$ is the horizontal wave vector. The HKE spectrum per unit volume is defined as

$$E_{\mathrm{h}}(\mathrm{k}) \coloneqq \frac{1}{2}\bar{\rho}[\widehat{u}(\mathbf{k})\widehat{u}(\mathbf{k}) + \widehat{v}(\mathbf{k})\widehat{v}(\mathbf{k})], \tag{1}$$

where $\bar{\rho}$ is the height-variant basic state density and $\mathbf{u} = (u, v)$ is the horizontal wind velocity vector. According to Peng *et al.* (2015a; 2015b) and Zheng *et al.* (2020), the spectral energy budget can then be written as

$$\begin{aligned}\partial_{\mathrm{t}}E_{\mathrm{h}}(\mathbf{k}) = {} & C_{\mathrm{A}\to\mathrm{h}}(\mathbf{k}) + \partial_z F_{\mathrm{p}\uparrow}(\mathbf{k}) + t_{\mathrm{h}}(\mathbf{k}) + \partial_z F_{\mathrm{h}\uparrow}(\mathbf{k}) \\ & + D_{\mathrm{h}}(\mathbf{k}) + J_{\mathrm{h}}(\mathbf{k}) + H_{\mathrm{h}}(\mathbf{k}) + \mathrm{D}is_{\mathrm{h}}(\mathbf{k}),\end{aligned} \tag{2}$$

where $\partial_{\mathrm{t}}E_{\mathrm{h}}(\mathbf{k})$ is the net tendency term of the HKE. $C_{\mathrm{A}\to\mathrm{h}}(\mathbf{k})$ is indicative of the spectral conversion from APE to HKE; that is, the conversion term. $F_{\mathrm{h}\uparrow}(\mathbf{k})$ and

$F_{p\uparrow}(\mathbf{k})$ represent the vertical fluxes of HKE and pressure respectively; therefore, $\partial_z F_{h\uparrow}(\mathbf{k})$ and $\partial_z F_{p\uparrow}(\mathbf{k})$ are the vertical flux divergence terms. $t_h(\mathbf{k})$ is the nonlinear spectral transfer term. $D_h(\mathbf{k})$ represents the spectral tendency due to three-dimensional divergence. $H_h(\mathbf{k})$ is the spectral tendency due to diabatic processes. $J_h(\mathbf{k})$ and $\mathrm{Dis}_h(\mathbf{k})$ are the adiabatic non-conservative and dissipative terms respectively. The detailed expressions for the terms in Equation (2) can be written as follows:

$$C_{A\to h}(\mathbf{k}) = -c_p\overline{\rho}\overline{\theta}\widehat{w}\partial_z\widehat{\pi'}, \tag{3}$$

$$F_{p\uparrow}(\mathbf{k}) = -c_p\overline{\rho}\overline{\theta}\widehat{w}\widehat{\pi'}, \tag{4}$$

$$\begin{aligned} t_h(\mathbf{k}) = &-\overline{\rho}\widehat{\mathbf{u}}\cdot\mathrm{DCT}[\mathbf{u}\cdot\nabla\mathbf{u} + \mathbf{u}\nabla\cdot\mathbf{u}/2)] \\ &+\overline{\rho}\left\{\partial_z\widehat{\mathbf{u}}\cdot\mathrm{DCT}[w\mathbf{u}] - \widehat{\mathbf{u}}\cdot\mathrm{DCT}\left[w\partial_z\mathbf{u}\right]\right\}/2, \end{aligned} \tag{5}$$

$$F_{h\uparrow}(\mathbf{k}) = -\overline{\rho}\widehat{\mathbf{u}}\cdot\mathrm{DCT}[w\mathbf{u}]/2, \tag{6}$$

$$D_h(\mathbf{k}) = -\overline{\rho}\widehat{\mathbf{u}}\cdot\mathrm{DCT}\left[\mathbf{u}(\partial_z w + \nabla\cdot\mathbf{u})\right]/2, \tag{7}$$

$$J_h(\mathbf{k}) = -F_{h\uparrow}(\mathbf{k})\partial_z\ln\overline{\rho}, \tag{8}$$

$$H_h(\mathbf{k}) = c_p\overline{\rho}\widehat{H}_m\widehat{\pi'}, \tag{9}$$

$$\mathrm{Dis}_h(\mathbf{k}) = \overline{\rho}\widehat{\mathbf{u}}\cdot\widehat{\mathrm{Dis}}_u, \tag{10}$$

where $\widehat{f} = \mathrm{DCT}[f]$, representing f any of the variables/term in the equations, ∇ is the horizontal gradient operator, w is the vertical velocity, c_p is the specific heat of dry air at constant pressure, $\bar{\theta}$ is the height-variant basic-state potential temperature, $\pi' = \pi - \overline{\pi} = (p/p_0)^{R_d/c_p} - \left(\overline{p}/p_0\right)^{R_d/c_p}$ is the perturbed Exner pressure, with p, p_0, and $\overline{p}$ denoting pressure, reference surface pressure, and basic-state pressure respectively, and R_d is the gas constant for dry air. Also, $H_m = (1 + 1.61q_v)S_\theta + 1.61\theta S_{q_v}$ is the combined diabatic contributions, with q_v the water vapour mixing ratio, θ the potential temperature, and S_θ and S_{q_v} the diabatic contributions to $d\theta/dt$ and dq_v/dt respectively. Finally, Dis_u represents the dissipation of the horizontal velocity vector.

There is a consideration to be made on the dissipative term, $\mathrm{Dis}_h(\mathbf{k})$. It is impossible to properly define Dis_u from the output of semi-Lagrangian (HAR) and Eulerian (WRF) models (Becker, 2001). Thus, $\mathrm{Dis}_h(\mathbf{k})$ is derived following the methodology defined by Boville and Bretherton (2003) as the kinetic energy tendency considering the specific force from the diffusion process. A priori, it would be easier just to calculate $\mathrm{Dis}_h(\mathbf{k})$ as the difference of $\partial_t E_h(\mathbf{k})$ with the summatory of every other term (Equations 3–9). However, this would reflect not only the physical dissipation, but also the numerical dissipation imposed by the limited-area model and the energy inputs by the initial/boundary conditions.

The discussion about $\partial_z F_{h\uparrow}(\mathbf{k})$ and $\partial_z F_{p\uparrow}(\mathbf{k})$ will also include the $F_{h\uparrow}(\mathbf{k})$ and $F_{p\uparrow}(\mathbf{k})$. In these cases, the vertical evolution of both terms allows us to understand the relative contributions within all the terms included in Equation (2). However, to describe the behaviour of these two particular terms on the energy budget, it is much easier and more straightforward to consider the vertical fluxes instead of their vertical evolution (Zheng *et al.*, 2020). It is also worth noting that, to be methodologically accurate, the direction of the energy cascade should be expressed as the accumulation of the HKE transfer from nonlinear interactions, defined by Peng *et al.* (2015a) as

$$\prod_h(k_h) = \sum_{k\geq k_h} t_h(K)\Delta k. \tag{11}$$

This has been the computation used to discuss the results of upscale and downscale propagations of t_h; however, the figures are not shown for the sake of simplicity (Supporting Information Figures S6 and S7).

The spectral budget gives an exhaustive evaluation of the HKE dynamics and shows possible sources and sinks driving the energy cascade. Thus, to explore a better understanding of how the NWP models behave in the simulation of TTs, a case study is selected, the TT of Tropical Storm *Delta*. The different terms of Equation (2) are obtained from every tropospheric level of the HAR and WRF simulations of this TT. These are averaged over 24 hr, covering ±12 hr around the time of transition. The results are depicted as a vertical distribution along the wave-numbers range, for both synoptic scale and mesoscale. Please note that the spectral HKE budget results are shown on a logarithmic scale to facilitate the comparison among the diverse term contributions.

3 | RESULTS AND DISCUSSION

In this section, the HKE spectra of the most intense TTs evaluated by Calvo-Sancho *et al.* (2022) are shown, followed by the assessment of the spectral budget of Tropical Storm *Delta* as a case study. For the spectral budget, we have chosen to present the full vertical distribution of the results. However, most of the related literature shows theirs vertically averaged. Thus, to ease the comparison with the references mentioned, the Supporting Information includes vertically averaged results of the

spectral HKE budget terms in three tropospheric layers: low (surface to 850 hPa), middle (700–500 hPa), and upper troposphere (450–250 hPa).

3.1 | HKE spectra

Early results for this study showed that the simulations produce a steeper HKE spectrum at higher tropospheric levels, whereas the lower levels generate shallower curves. This is mainly noticed in the synoptic range, and it has already been mentioned by Bolgiani *et al.* (2022), presenting results in line with Skamarock (2004). This is as expected, as jet streams and planetary-scale waves belong to upper levels and the higher synoptic energy density steepens the curve. The results for several pressure levels were initially evaluated (not shown) and finally the 500 hPa HKE spectra are considered as the most representative for this work.

3.1.1 | WRF energy assimilation and model resolution

The energy spectrum simulated is directly related with the grid resolution of the NWP model (Skamarock, 2004). This can be clearly seen in the ability of the models to reproduce the transition from k^{-3} to $k^{-5/3}$ when resolution is increased (Abdalla *et al.*, 2013). The differences in energy assimilation from initial/boundary conditions, and its later management by the model, are especially noteworthy in finite-differences models, as WRF. Figure 1 shows the 500 hPa wind HKE spectra for the averaged (42 hr before to 30 hr after the TT) simulation of each of the four TTs simulated with WRF at their respective D01 and D02. As a reference of the energy levels "fed" to the limited-area model, the ERA5 September–November climatology for the North Atlantic basin (Bolgiani *et al.*, 2022), with a resolution of 27.0 km, is also shown. It becomes immediately clear that each increase in resolution enhances the $k^{-5/3}$ transition in the curves, as expected by the Lindborg (1999, eq. 71) observations. The ERA5 initial and boundary conditions are properly reproducing the HKE for the synoptic scale, especially at $\lambda_h > 1{,}000$ km, but fall very short of the observed curve below 600 km. This is in line with Augier and Lindborg (2013), who found that the ECMWF Integrated Forecasting System model, on which the ERA5 is based, is very dissipative at synoptic scales, even to the point of not being able to feed the downscale energy cascade. Nevertheless, this is the information assumed by the WRF model at D01, which then yields a simulation with a much later decay of the curves; that is, the spectra reproduce the transition to the mesoscale slope and show a larger range of wavelengths reaching smaller scales. Thus, Figure 1 allows us to understand how the WRF model assimilates the energy information from the initial and boundary conditions and presents energy levels according to the resolution.

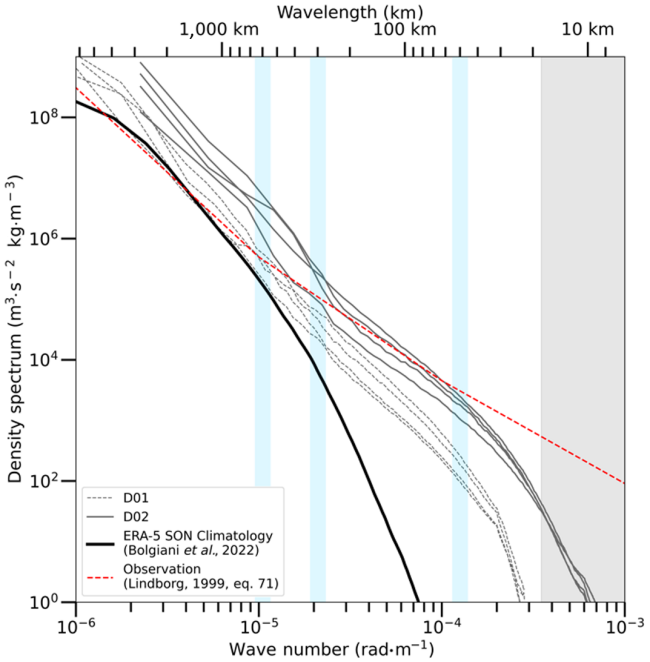

FIGURE 1 The 500 hPa wind horizontal kinetic energy spectra for the four tropical transitions simulated with Weather Research and Forecasting at their respective inner (D01) and outer domain (D02). The fifth generation of the European Centre for Medium-Range Weather Forecasts Atmospheric Reanalysis (ERA5) September–November (SON) climatology and the observed energy horizontal wave-number spectral curve are shown for reference. The shaded area corresponds to the wavelengths below the theoretical effective resolution of D02, computed according to Skamarock (2004). Vertical shaded bands (blue) indicate the wavelength at which the spectra deviate from the expected curves. [Colour figure can be viewed at wileyonlinelibrary.com]

The D01 spectra simulated by the high-resolution model (Figure 1) are more adequate than the ERA5 spectrum for the transition into mesoscale, down to $\lambda_h \approx 300$ km, but do not properly capture the shallower spectral curve slope rates of the mesoscale. This is clearly done by D02, simulating a set of spectra very well adjusted to the mesoscale down to $\lambda_h \approx 40$ km. To avoid any confusion by the reader, it must be noted that the spectra are corrected by density, as they correspond to 500 hPa HKE, and this drives the final point of the curves above the $2\Delta x$ expected by Nyquist (1928). Also, there is a notable difference in energy between D01 and D02 all along the spectra. There is very scarce literature about this effect; however, at finer resolutions, the simulations consider a

larger amount of energy (Rai *et al.*, 2017), as more grid points can be computed in the same area, producing the parallel shift of the curves upwards. Similar results were already noted by Bolgiani *et al.* (2020) as well as in previous studies using WRF (Skamarock, 2004) and HAR (Abdalla *et al.*, 2013). The effect is much less noticeable for spectral models (Abdalla *et al.*, 2013) owing to the mathematical approach. However, it is not negligible, as limited-area spectral models require the simulation of a periodic domain to handle the spectrum. This is done in the form of a lateral buffer zone around the domain boundaries, which creates a toroidal shape rendering the limited domain into a periodic one (Seity *et al.*, 2011). This enables one to simulate the complete spectral wavelength, which may introduce some errors in the computations. The parallel shift makes each resolution to be more adequate for a certain wavelength range when compared with the Lindborg (1999, eq. 71) spectrum.

The results of Figure 1 are in line with Skamarock (2004), who proves that the energy assimilation of the NWP model depends on the resolution, which should be adapted to the specific horizontal scale to study. In accordance with this, the spectra for WRF D02 tend to be overenergized in the synoptic scale, with a spectral curve slope rate a little larger than k^{-3} in general terms. The transition to $k^{-5/3}$ rate is sharper than expected by Lindborg (1999, eq. 71), followed by a steeper curve in the mesoscale, albeit that the HKE density levels are very adequate down to $\lambda_h \approx 40$ km. The TTs also present large differences at synoptic scale, which are notably reduced as the curves get into smaller wavelengths, where the resolution is more adequate.

3.1.2 | WRF and HARMONIE model comparison

Figure 2 presents the spectra simulated by WRF D02 and HAR for the four TTs selected (Table 1). The results show that HAR consistently produces a lower HKE than WRF in synoptic scale and mesoscale, most marked for $\lambda_h < 40$ km. This is an indication that the numerical dissipation (filtering) is steeper by this model. Nonetheless, it is noteworthy that the HAR spectra match and even surpass the WRF spectra energy density levels at some point in the mesoscale for every case, usually at $\lambda_h \approx 200$ km.

The results for the TT of *Delta* and *Theta* (Figure 2) are very similar for both models. They show that these events are clearly very energetic, presenting spectra above the Lindborg curve down to $\lambda_h \approx 60$ km. This generates a steeper than expected spectral curve slope rate for both models and both cases, which makes it difficult to appreciate the rate transition to $k^{-5/3}$. On the other hand, this steeper curve indicates that the predictability of these high-energy systems is unlimited ($p \geq 3$) for the synoptic flow characteristics (Lorenz, 1969; Zheng *et al.*, 2020), becoming limited ($p < 3$) for the meteorological features below $\lambda_h \approx 200$ km. *Ophelia* presents a spectrum that would indicate a lower predictability at synoptic scales, as the spectra seem to be shallower than the k^{-3} curve. Also, the HKE density levels for $\lambda_h < 40$ km clearly lie below the observed curve for the four TTs, indicating that the energy of the fine convective processes might not be properly reproduced to the full extent of the atmospheric conditions. This is a very important question to address, as we are evaluating one of the most convective and latent-heat-dependent atmospheric events. It would also be in line with the study by Quitián-Hernández *et al.* (2021), who conclude that HAR consistently underestimates the cloudiness in tropical cyclones simulations.

The results for TT *Leslie* (Figure 2) produce an overenergetic atmospheric situation down to $\lambda_h \approx 60$ km; however, the spectral curve slope rate is shallower than expected for $1{,}000 > \lambda_h > 400$ km, with a notable steepening at $\lambda_h \approx 300$ km and a $k^{-5/3}$ rate starting just above $\lambda_h = 200$ km. Something similar, albeit at smaller wavelengths, was already noted by Vonich and Hakim (2018), who attributed the effect to the higher wind speed and vorticity of a tropical storm. They consider the Coriolis effect to be partially responsible, suggesting that shallower rates are generic to tropical environments, but this might not be the case for our TTs (see Table 1 latitudes). The results are also in line with Wang *et al.* (2018), who present a notable steepening of the curve at similar wavelengths, which they relate to the cyclone scale. *Ophelia* presents this steepening at $\lambda_h \approx 400$ km. In the cases of *Delta* and *Theta*, this "bulge" in the spectrum is not as clear, due to the overenergetic synoptic scale; however, both gain the mesoscale spectral curve slope rate at $\lambda_h < 200$ km. This "hump" effect in the mesoscale slope is related to the TT maximum wind speed (Table 1), in line with the results by Zheng *et al.* (2020), who conclude that the HKE spectra show a $k^{-5/3}$ slope over the central mesoscale with a "swelling" at larger wavelengths, finding that the transition zone between the two areas shifts downscale as the storm intensity increases. Wang *et al.* (2018), as well as Vonich and Hakim (2018), also consider that the increased HKE ("arc-like shape") they see in the middle–upper troposphere spectra is characteristic of tropical cyclones, mainly due to vorticity and convection, with a distinctive peak at $\lambda_h \approx 500$ km.

It must be pointed that there are notable differences between the models in the $600 > \lambda_h > 60$ km range for TT

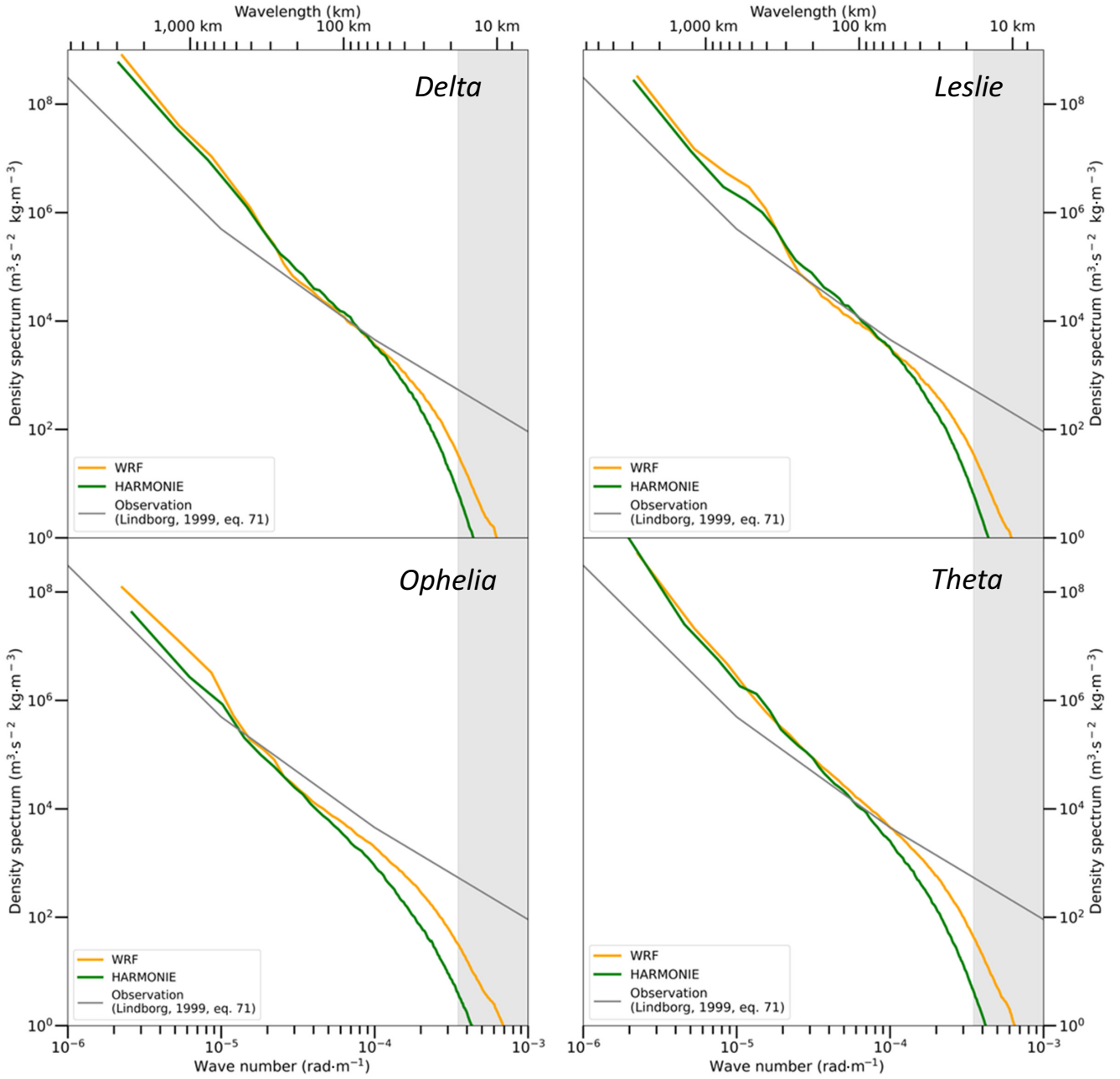

FIGURE 2 The 500 hPa wind horizontal kinetic energy spectra for the tropical transition selected, simulated with Weather Research and Forecasting (WRF; outer domain, D02) and HARMONIE. The observed energy horizontal wave-number spectral curve is shown for reference. The shaded area corresponds to the wavelengths below the theoretical effective resolution of the models (computed according to Skamarock, 2004). [Colour figure can be viewed at wileyonlinelibrary.com]

Leslie. WRF energy density is larger near the synoptic scale but shows a major decrease just above $\lambda_h \approx 200$ km. Below this wavelength, the HAR spectrum is more energetic, remaining over the observed curve, while WRF underestimates the atmospheric HKE. Nonetheless, the major differences between the simulations are shown for TT *Ophelia* (Figure 2). In this case, WRF is consistently more energetic than HAR at synoptic scale and mesoscale, just momentarily presenting the same HKE density at $\lambda_h \approx 200$ km. The WRF spectrum is below the Lindborg curve at every point in the mesoscale, whereas HAR seems to be unable to even capture the $k^{-5/3}$ spectral curve slope rate. These results can be related with the aforementioned predictability of the spectra, linked to the k^{-p} power-law behaviour. In all, it is clear from the results that the behaviour of the TTs can present significant variations in the HKE spectra and that the NWP models struggle to properly reproduce it at some wavelength ranges.

3.2 | Case study: TT of Tropical Storm *Delta*

As mentioned in the previous section, the HKE spectrum produced by Tropical Storm *Delta* is representative of a high-energy configuration at middle tropospheric levels. This storm is also the second most intense of those selected in this study with regard to maximum sustained wind speed and sea-level pressure (Table 1). Moreover, Bolgiani *et al.* (2022) already used this event as an example to compare with the ERA5 HKE spectra climatology. Thus, the TT of *Delta* is selected here as a case study to evaluate the energy spectral budget.

3.2.1 | Synoptic situation

Tropical Storm *Delta* had a severe impact on the Canary Islands archipelago in November 2005, producing several casualties and many injuries, flooding, landslides, power outages, and major economic losses. The system generated southwest of the Azores Islands on November 19, 2005, and reached subtropical cyclone characteristics 3 days later. The storm experienced a TT into tropical storm status on the November 23, 2005, and continued intensifying until November 28. It finally decayed into an extratropical storm with a warm core (Sanchez-Laulhe and Martin, 2006). Increased rainfall and wind intensity were observed on the Canary Islands prior to the effects of *Delta* (Seco *et al.*, 2009).

At the time of the transition, the atmospheric configuration (Figure 3) is characterized by an upper level cut-off low around 30°N 040°W, and *Delta* as an isolated deep fully diabatic warm-core cyclone. The potential vorticity is redistributed vertically by an important release of latent heat (e.g., differential diabatic heat source; not shown), which favours the final development of a tropical cyclone purely governed by diabatic processes (Bolgiani *et al.*, 2022; Calvo-Sancho *et al.*, 2022). On the surface (Figure 3b), the wind field presents asymmetry at the instant of the TT (Calvo-Sancho *et al.*, 2022), with values exceeding 19 $m \cdot s^{-1}$ in the northwestern quadrant, sustained winds around 16 $m \cdot s^{-1}$ in the centre, and lower values in the southeast quadrant of the system. At 500 hPa (Figure 3c), the wind-speed values are remarkably larger than the surface winds, clearly reinforced by a jet stream located on the western area of the cyclone. This vertical wind configuration, common in cyclones that experience a TT process, depicts a wind-speed reduction with height for the lower troposphere (not shown) and an increased cyclonic wind in the middle troposphere, sustained by a jet. In addition, deep convection dominates at the instant of the TT (Figure 3d) and favours latent heat release, which promotes the vertical redistribution of the potential vorticity (Calvo-Sancho *et al.*, 2022), contributing to an increase in low-level vorticity. This atmospheric configuration is representative of a high-energy state in the middle levels of the atmosphere, as expected for a tropical cyclone with baroclinic genesis, mainly forced by the jet stream present at 500 hPa (Figure 3c).

3.2.2 | Spectral budget

To gain more insight into the dynamics of the HKE spectra, the different processes that contribute to the tropospheric energy evolution and transference in TT *Delta* are analysed here. First, it is noteworthy that the evaluation of the HKE tendency $\partial_t E_h(\mathbf{k})$ presents a strong energy input for $2{,}500 > \lambda_h > 800$ km, followed by a plateau and a moderate decrease of energy at $400 > \lambda_h > 100$ km (not shown). The behaviour is similar for both models, although HAR presents more energy at the mesoscale tendency. In the following we individually analyse the vertical distribution of all the terms in Equation (2) produced by the WRF and HAR simulations for the synoptic scale and mesoscale.

Term $C_{A\to h}(\mathbf{k})$. This term accounts for the buoyancy forcing, determined by the energy conversion from APE to HKE. The $C_{A\to h}$ contributions to HKE are moderate in general and almost identical for HAR and WRF. At the synoptic scale (Figure 4), both models present negative to neutral values in the lower troposphere, indicating a conversion from HKE to APE. For the middle and upper troposphere, the buoyancy forcing is important for $\lambda_h > 2{,}000$ km, presenting high positive values, but is negligible for the lower wavelengths. These results can also be noted in the level-averaged $C_{A\to h}$ results (Supporting Information Figures S1 and S2). As the height increases, growing values are found for the large scales, whereas the opposite behaviour is found for small wavelengths.

The distribution seems to be inverted at the mesoscale (Figure 5), with negative values for the middle and upper troposphere and a contribution from APE to HKE in the lower troposphere and the stratosphere. The positive $C_{A\to h}$ values for the low levels could be related to the direct forcing of APE by the latent heating, of major importance in these kinds of system (Calvo-Sancho *et al.*, 2022). Similar results in the tropospheric $C_{A\to h}$ behaviour are shown by Peng *et al.* (2015a; 2015b), who studied the spectral energy budget associated with WRF baroclinic wave simulations and indicated that the energy conversion of APE to HKE is mainly promoted by moist processes, which take place at all the mesoscale and synoptic wavelengths below 1,000 km. Sun *et al.* (2017) simulate convective

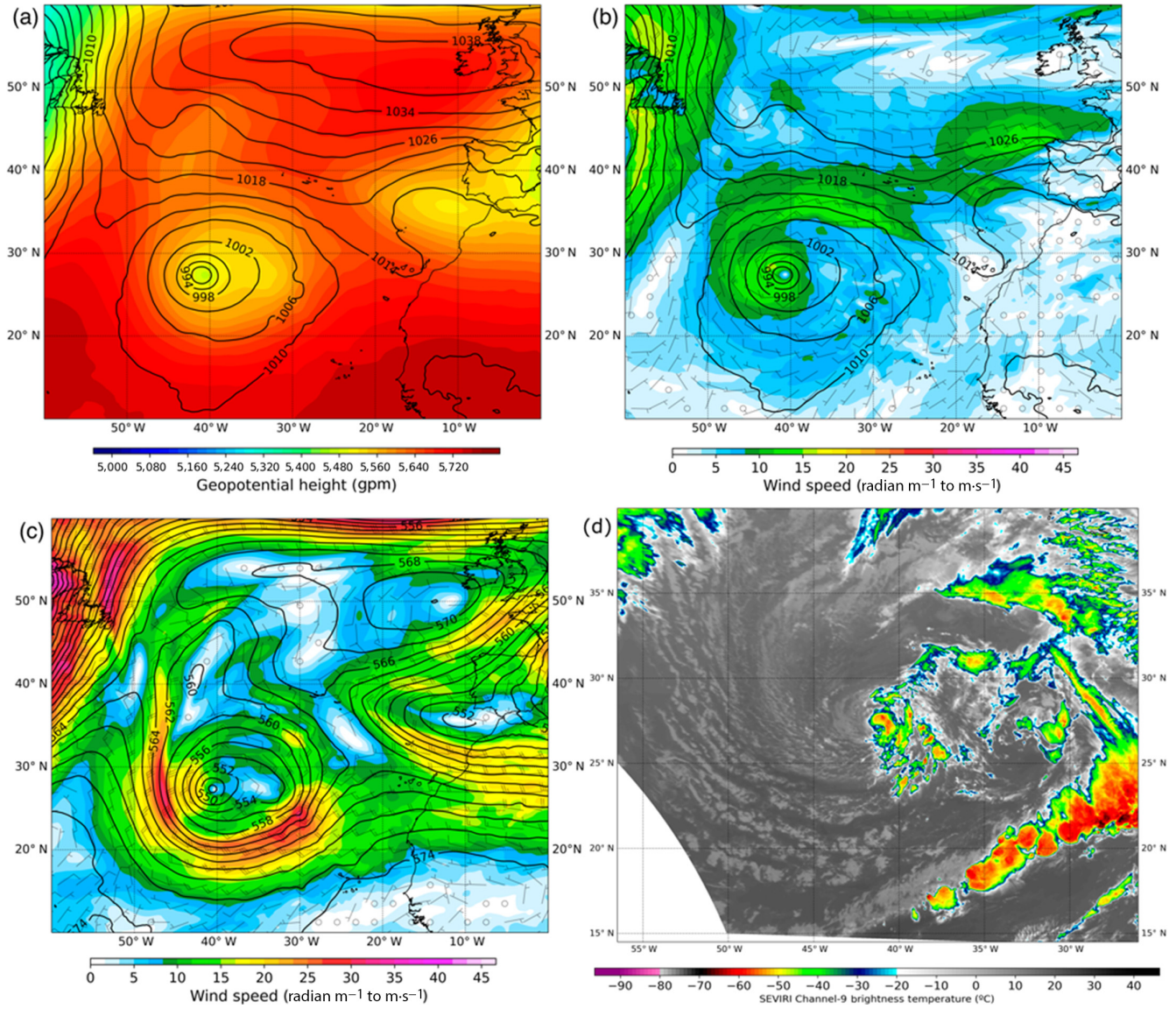

FIGURE 3 (a) Mean sea-level pressure (hPa, contours) and 500 hPa geopotential height (gpm, shaded); (b) surface wind speed ($m \cdot s^{-1}$, shaded) and direction (barbs), and mean sea-level pressure (hPa, contours); (c) 500 hPa wind speed ($m \cdot s^{-1}$, shaded) and direction (barbs), and 500 hPa geopotential (gpm, contours); and (d) SEVIRI channel-9 brightness temperature (°C, shaded) for Tropical Storm *Delta* on November 23, 2005, 1200 UTC. [Colour figure can be viewed at wileyonlinelibrary.com]

systems, also with WRF, revealing small buoyancy effects with $C_{A\to h}$ positive values at low tropospheric levels for $\lambda_h > 50$ km, because of the downdrafts promoted by the evaporative cooling in midlevels. Also, Calvo-Sancho *et al.* (2022) evaluate several TTs in the Atlantic Ocean, finding a large release of latent heat in the hours before the transition. This increases the low-level potential vorticity and intensifies the circulation around the centre of the cyclone in the lower troposphere. In the results here shown, this effect is reflected in the low-level band of positive $C_{A\to h}$ values found for both HAR and WRF, indicating an APE to HKE conversion for all mesoscale wavelengths.

Term $\partial_z F_{p\uparrow}(\mathbf{k})$. This term takes into account the pressure vertical flux divergence, which can transfer HKE through the propagation of inertial gravity waves (IGWs) generated by moist convection outburst (Peng *et al.*, 2015b). Once convection has developed in the system, the pressure vertical flux reflects the upward ($F_{p\uparrow} < 0$) or downward ($F_{p\uparrow} > 0$) propagation of tropospheric IGWs, influencing the HKE spectrum across the vertical levels. The $\partial_z F_{p\uparrow}(\mathbf{k})$ contributions are moderate and similar for both models in the troposphere, albeit that they show notable differences in stratospheric levels (Figures 4 and 5). At the synoptic scale, the $\partial_z F_{p\uparrow}(\mathbf{k})$ shows values entirely positive from 2,500 m up to 10,000 m at every

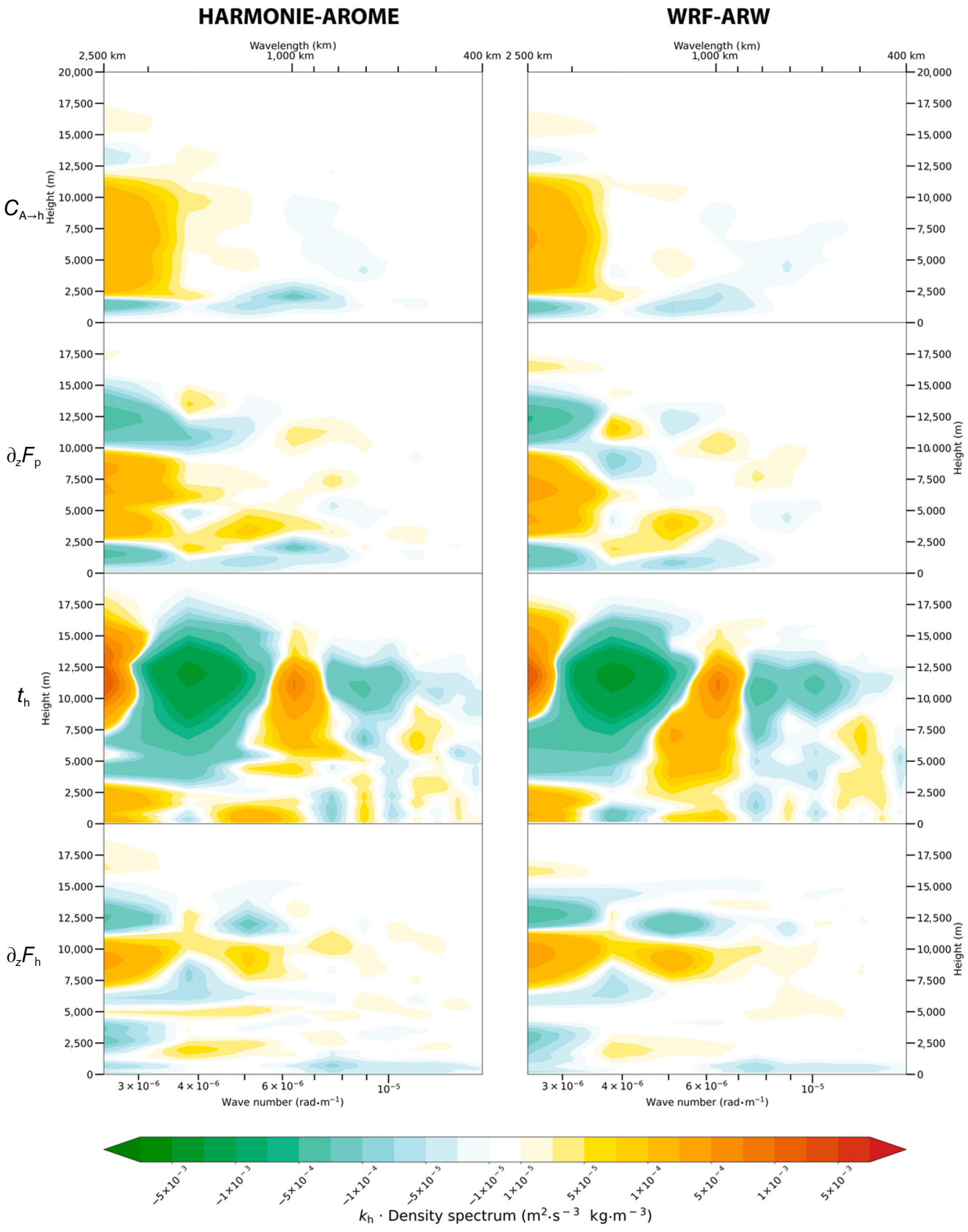

FIGURE 4 Vertical distribution of horizontal kinetic energy spectrum budget ($m^2 \cdot s^{-3} \cdot kg \cdot m^{-3}$) at synoptic scale for the HARMONIE-AROME and WRF simulations. The terms shown correspond to Equations 3–6 from top to bottom respectively. Note that the spectra are shown on a log scale to facilitate the comparison between the contributions of each term. [Colour figure can be viewed at wileyonlinelibrary.com]

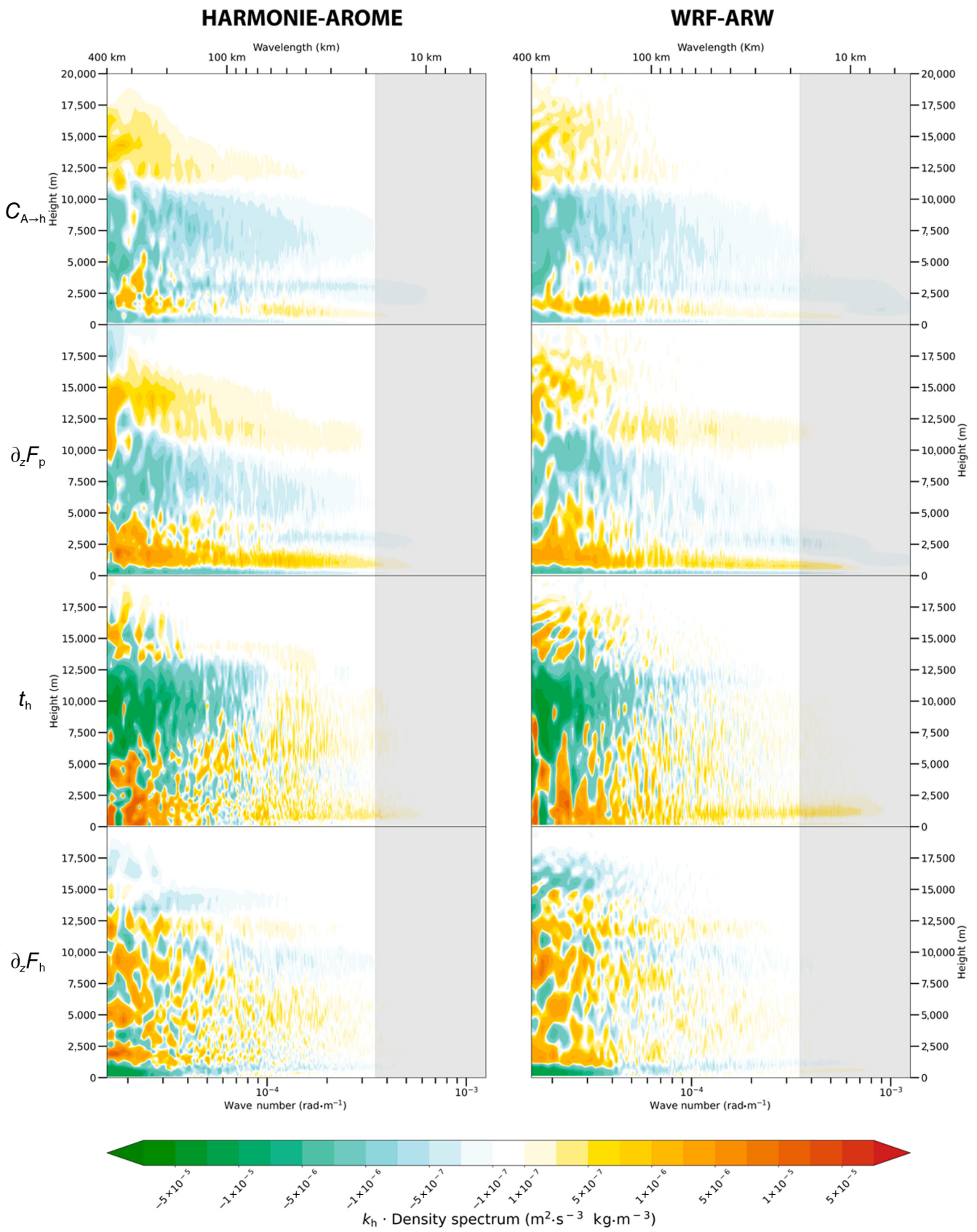

FIGURE 5 As Figure 4 except for mesoscale for the HARMONIE-AROME and Weather Research and Forecasting (WRF) simulations. ARW: Advanced Research WRF. Note that the limits of the colour bar are different from Figure 4. [Colour figure can be viewed at wileyonlinelibrary.com]

wavelength and mostly negative for the remaining layers (Figure 4), indicating that the HKE is carried away from the middle–upper troposphere by IGWs and deposited into the rest of the layers. The $F_{p\uparrow}$ results (Figure 6) for low tropospheric levels present negative values at every wavelength, indicating an upward motion taking HKE and transferring it to upper levels due to wave propagation. From 5,000 m to the tropopause and $\lambda_h > 1{,}000$ km, the general rule seems to be the downward flux, representing a transfer of HKE into the lower troposphere. This is not the case for $1{,}000 > \lambda_h > 600$ km. Between these wavelengths, typical for tropical storm diameters (Wang *et al.*, 2018), negative values are found for all of the troposphere, suggesting that the IGWs propagate all the way into the stratosphere, taking HKE into higher levels. At stratospheric levels, the results differ between the models. Whereas WRF presents an upward transfer of HKE for every wavelength, HAR shows a downward flux for $\lambda_h < 1{,}500$ km. Nonetheless, the stratosphere is where the vertical resolution most differs between the models, so we should be cautious about these results.

At the mesoscale, the $\partial_z F_{p\uparrow}(\mathbf{k})$ shows negative values at the middle–upper levels at every wavelength (Figure 5), more clearly shown in the HAR results, and mostly positive in the remaining levels, denoting a transfer of HKE by IGWs from the lower troposphere and lower stratosphere to the middle troposphere. The mesoscale $F_{p\uparrow}$ flux results (Figure 6) present the same near-surface layer of upward flux as for the synoptic scale, albeit thinner. The middle troposphere is dominated by the downward $F_{p\uparrow}$ flux at every wavelength between 2,000 and 5,000 m, whereas the upper troposphere is again showing upward values. The WRF results show a stratosphere dominated by upward fluxes again, but HAR presents positive values above 15,000 m.

Additionally, the results averaged over the three tropospheric layers (Supporting Information Figures S1 and S2) show positive values in middle tropospheric levels at the largest wavelengths for both models, indicating a deposit of HKE. The latent heating derived from the moist processes of the TTs increases the IGW activity, enhancing the transfer of HKE to the middle troposphere, mainly from lower levels, highlighting the role of moist convection outbursts, characteristic of the TT events (Calvo-Sancho *et al.*, 2022). This behaviour of $F_{p\uparrow}$ is consistent with Durran and Weyn (2016), who conclude that the mesoscale spectrum slope can be derived solely from convection, which would explain the orders of magnitude that this term presents, rendering it a major variable for the formation of the HKE spectrum.

Term $t_h(\mathbf{k})$. This term accounts for the transfer of HKE among different horizontal scales in the spectrum, promoted by nonlinear interactions. It denotes the role of the energy cascade effect on the HKE budget, as a result of a direct ($\Pi_h(k_h) > 0$; downscale) or indirect ($\Pi_h(k_h) < 0$; upscale) propagation of energy. The contributions by t_h are strong and very similar for both models. For the synoptic scale (Figure 4), the energy cascade results are significant for the larger wavelengths with a succession of alternating values in two differentiated layers and almost neutral for $\lambda_h < 500$ km. For the levels below 2,500 m the downscale propagation is predominant ($\Pi_h(k_h) > 0$), whereas in the middle and upper troposphere the HKE cascade seems to flow mainly upscale ($\Pi_h(k_h) < 0$). This may be partially related to the conclusions of Lindborg (2005) on quasi-geostrophic dynamics, which show that strong rotation in the flow may produce an inhibition of the direct cascade, accumulating energy at larger scales than the distinctive wavelength of the storm, which is $\lambda_h \approx 500$ km (critical Rossby number ≈0.1; Lindborg, 2005), from the results in Section 3.1. Thus, the results for TT *Delta* present a nonlinear transmission of HKE that can run in both directions, in contradiction with the classical Kolmogorov (1941) cascade theory, and in line with the findings by Wang *et al.* (2018), who conclude that any cascade theory alone is insufficient to explain the formation of the spectra below the distinctive wavelength of tropical cyclones.

The mesoscale results (Figure 5) show a behaviour dependent on the vertical levels, in line with the results by Sun *et al.* (2017). Below 5,000 m the direct cascade is predominant ($\Pi_h(k_h) > 0$), whereas the upper troposphere is dominated by an indirect ($\Pi_h(k_h) < 0$) flow of energy for the larger wavelengths and direct ($\Pi_h(k_h) > 0$) for the lower ones. This upscale transference might be related to the forcing of HKE by tropical storms, as noted by Vonich and Hakim (2018), Wang *et al.* (2018), and Zheng *et al.* (2020), who conclude that these types of event can influence the synoptic spectral curve slope rate of the spectra, producing a slope steeper than $k^{-5/3}$ at large mesoscale wavelengths. For $\lambda_h < 60$ km, the effect of t_h is almost negligible.

The vertical averages of this term (Supporting Information Figures S1 and S2) present mostly positive values for the synoptic scale at lower and middle levels, indicating a direct HKE cascade (Supporting Information Figures S6 and S7). The upper troposphere, however, shows an area of large negative values at $\lambda_h \approx 2{,}000$ km, indicating an upscale energy transport. This behaviour is also shown at middle tropospheric levels in the mesoscale.

Term $\partial_z F_{h\uparrow}(\mathbf{k})$. This term is the vertical flux divergence, and it is associated with the vertical transportation of moist convection. The HKE vertical flux $F_{h\uparrow}$ indicates the vertical upward ($F_{h\uparrow} < 0$) or downward ($F_{h\uparrow} > 0$) propagation transport of energy due to moist convection. The $\partial_z F_{h\uparrow}(\mathbf{k})$ contributions are moderate and similar for both models

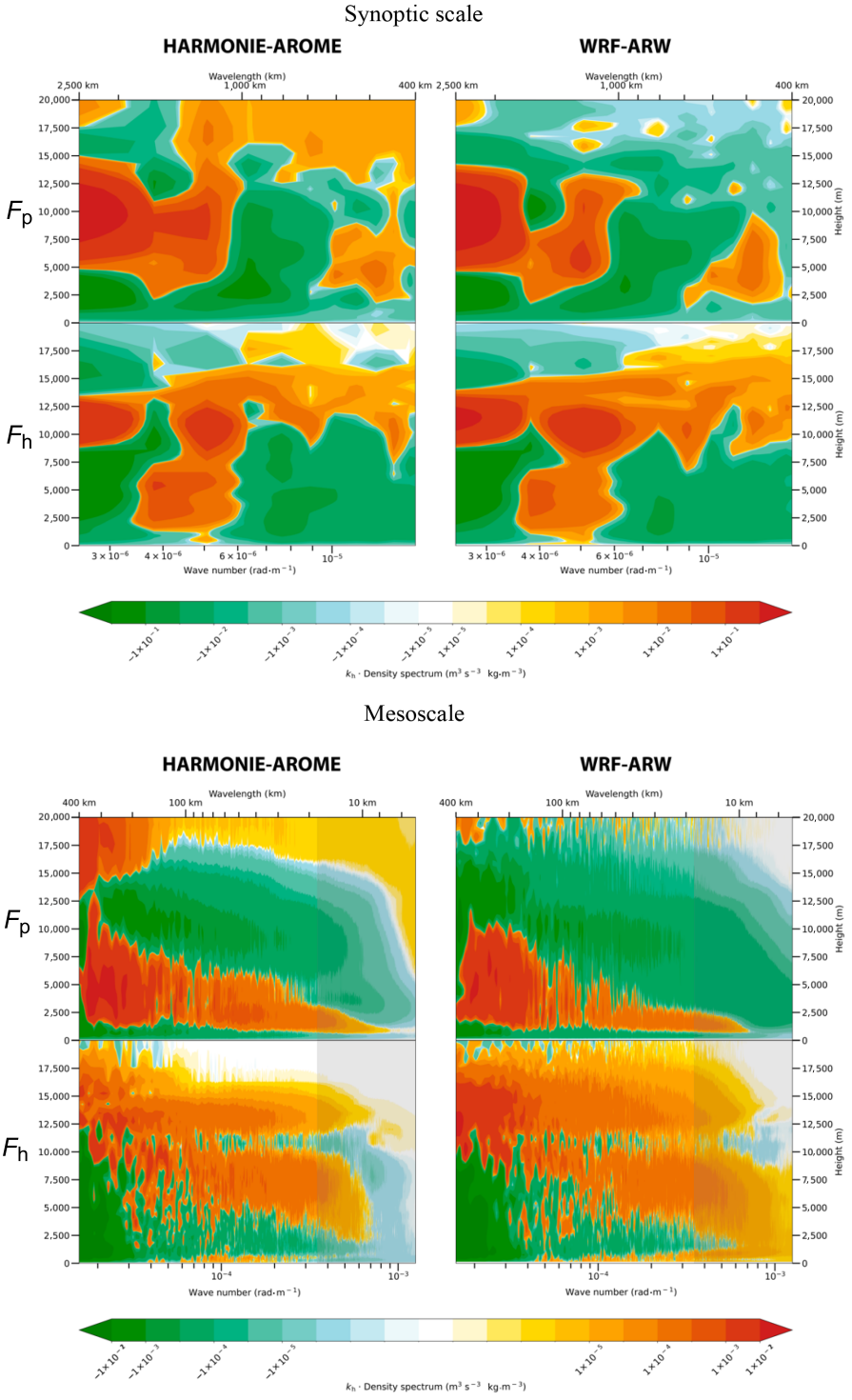

FIGURE 6 Distribution of the vertical fluxes of horizontal kinetic energy and pressure ($m^3 \cdot s^{-3} \cdot kg \cdot m^{-3}$) at synoptic scale (upper panels) and mesoscale (lower panels) for the HARMONIE-AROME and Weather Research and Forecasting (WRF) simulations. ARW: Advanced Research WRF. Note that the limits of the colour bar are different for the synoptic and mesoscale panels. [Colour figure can be viewed at wileyonlinelibrary.com]

at tropospheric levels (Figures 4 and 5). At the synoptic scale, $\partial_z F_{h\uparrow}(\mathbf{k})$ shows an overall positive contribution in the upper troposphere and negative contributions in the lower troposphere and stratosphere (Figure 4). The large-scale $F_{h\uparrow}$ results (Figure 6) show that the lower and middle troposphere are dominated by an upward transfer at all wavelengths except for $2{,}000 > \lambda_h > 1{,}000$ km, whereas downward values can be found for almost all the upper troposphere. Again, similar to the results of $F_{p\uparrow}$, this highlights that the energy budget is being governed by the convection and latent heat release associated with the TTs. The results are in line with the work by Wang *et al.* (2018), who concluded that the energy cascade theory is insufficient to explain the complete formation of the spectrum associated with tropical cyclones, and that moist convection, IGW propagation, and vertical fluxes must be taken

into account. In addition, Zheng *et al.* (2020) show that the various terms affect the whole vertical of the troposphere and are relatively similar among tropical cyclones.

In the mesoscale (Figure 6), the $F_{h\uparrow}$ results show a downward energy transport for the lower and middle troposphere, highlighting the role of convection and heat release. There are positive values associated with a downward transport in the middle–upper troposphere, possibly related to precipitation dragging effects (Zheng *et al.*, 2020). The results also present a notable difference between models in the stratosphere. Both simulations generate a downward flux, but WRF shows larger values at all wavelengths and levels, whereas HAR becomes neutral above 16,000 m for most of the spectrum. The averaged $\partial_z F_{h\uparrow}(\mathbf{k})$ (Supporting Information Figures S1 and S2).

It must be noted that $F_{h\uparrow}$ seems to behave in the opposite direction to $F_{p\uparrow}$ in the tropospheric mesoscale. This would indicate that the moist convection is transporting the HKE upwards in the lower troposphere, while counteracted in similar magnitudes by the energy transported by the propagation of the induced IGWs. When both terms are added into a single result (not shown) it reveals that there is not a full counterbalance and $F_{p\uparrow}$ seems to dominate. However, the addition of both terms for the synoptic scale (not shown) presents a dominance by $F_{h\uparrow}$, most notable at $\lambda_h < 1{,}000$ km, coincident with the typical tropical storm diameters. This might be explained by the latent heat release associated with the TTs, in line with Hamilton *et al.* (2008), who pointed out the significant contribution of these processes in the excitation and maintenance of the HKE.

Term $D_h(k)$. This term accounts for the spectral tendency due to the three-dimensional divergence. The contributions by D_h are strong in general and very similar for WRF and HAR. The divergence at synoptic ranges (Figure 7) shows a similar behaviour to t_h, with alternating values in the upper troposphere, presenting a large area of positive values at $\lambda_h \approx 1{,}500$ km. The results are also positive at higher tropospheric levels for the mesoscale (Figure 8), but become almost neutral for every level at $\lambda_h < 100$ km. The positive values of D_h indicate that the moist processes increase the three-dimensional divergence, inducing a positive contribution to APE in the upper levels (Peng *et al.*, 2014a). The results also reinforce the idea that a two-dimensional energy cascade, direct or indirect, is not enough to capture the full spectrum of a highly convective system like a TT and that strong connections between vertical levels exist, in accordance with Sun *et al.* (2017).

Term $J_h(\mathbf{k})$. This term represents the adiabatic non-conservative processes. The results of J_h are almost identical for both models, however, the contribution of this term is so weak that it does not provide any further insight on the behavior of the HKE spectra. If anything should be noted, it would be only a small negative contribution for the larger wavelengths of the tropospheric mesoscale is found (Figure 8). A significant contribution to mesoscale APE, also found by Peng *et al.* (2015b) in moist processes, is related to latent heat release. According to Peng *et al.* (2015b) and Wang *et al.* (2018), the combined contribution of D_h and J_h tends to be zero. This can be seen to a limited extent for the mesoscale, especially in the vertical averages (Supporting Information Figure S4). This balanced contributions by both terms would suggest that the flow at those layers is largely restricted by the anelastic approximation used in both WRF and HAR (Peng *et al.*, 2015b). However, this is clearly not the case for the synoptic results (Supporting Information Figure S3).

Term $H_h(\mathbf{k})$. This term takes into account the combined diabatic contributions to HKE. The contribution of H_h is strong and shows differences between the models, especially in the mesoscale. In the calculation of this term, two counteracting effects of moist processes are considered. On the one hand, the increase in atmospheric water vapour is directly related to the APE (Bannon, 2005). However, according to Pauluis and Held (2002), the moist processes involved in the TTs represent sources of latent heat, but, at the same time, they act as an atmospheric dehumidifier. The synoptic results (Figure 7) show alternating patterns of positive and negative results for the lower troposphere, and also for the middle and upper troposphere. WRF seems to produce more intense values, especially for the negative contributions in the stratosphere. In the mesoscale (Figure 8), WRF generates three distinct layers: a near-surface layer with negative contributions, a middle and upper tropospheric layer with positive values, and a negative stratosphere. HAR presents a similar but not that intense pattern, which become negligible at $\lambda_h < 100$ km, being a good example of the stronger numerical dissipation already noted in the evaluation of the HKE spectra. The vertical averages of H_h (Supporting Information Figures S3 and S4) make these differences between the two models more remarkable, showing opposite values at middle and upper levels.

Term $\mathrm{Dis}_h(\mathbf{k})$. This term represents the effect of the dissipative processes. The contributions of Dis_h are weak and very similar between the models. At the synoptic scale (Figure 7) there is a low-level layer of weak positive results at $\lambda_h > 1{,}000$ km, which may be the reflection of the heating produced by the frictional dissipation associated with surface stress (Boville and Bretherton, 2003). However, the most interesting feature is the large negative area in the upper troposphere, which indicates atmospheric cooling (Williamson, 2002; Boville and Bretherton, 2003) and may be the result of strong wind shear (Holtslag and Boville, 1993), as is the case for TT *Delta* (Calvo-Sancho

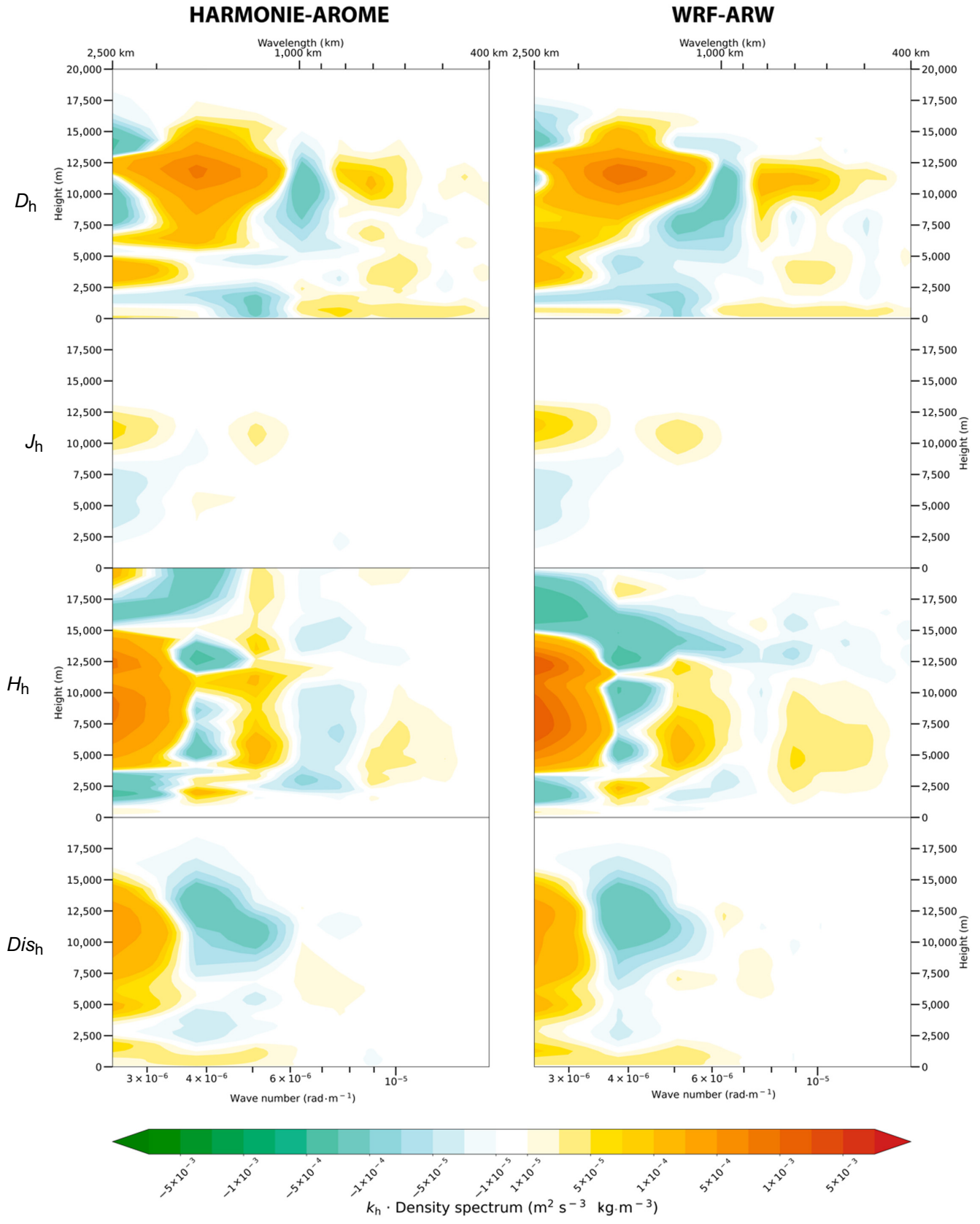

FIGURE 7 Vertical distribution of horizontal kinetic energy spectrum budget ($m^2 \cdot s^{-3} \cdot kg \cdot m^{-3}$) at the synoptic scale for the HARMONIE-AROME and Weather Research and Forecasting (WRF) simulations. ARW: Advanced Research WRF. The terms shown correspond to Equations 7–10 from top to bottom respectively. Note that the spectra are shown on a log scale to facilitate the comparison between the contributions of each term. [Colour figure can be viewed at wileyonlinelibrary.com]

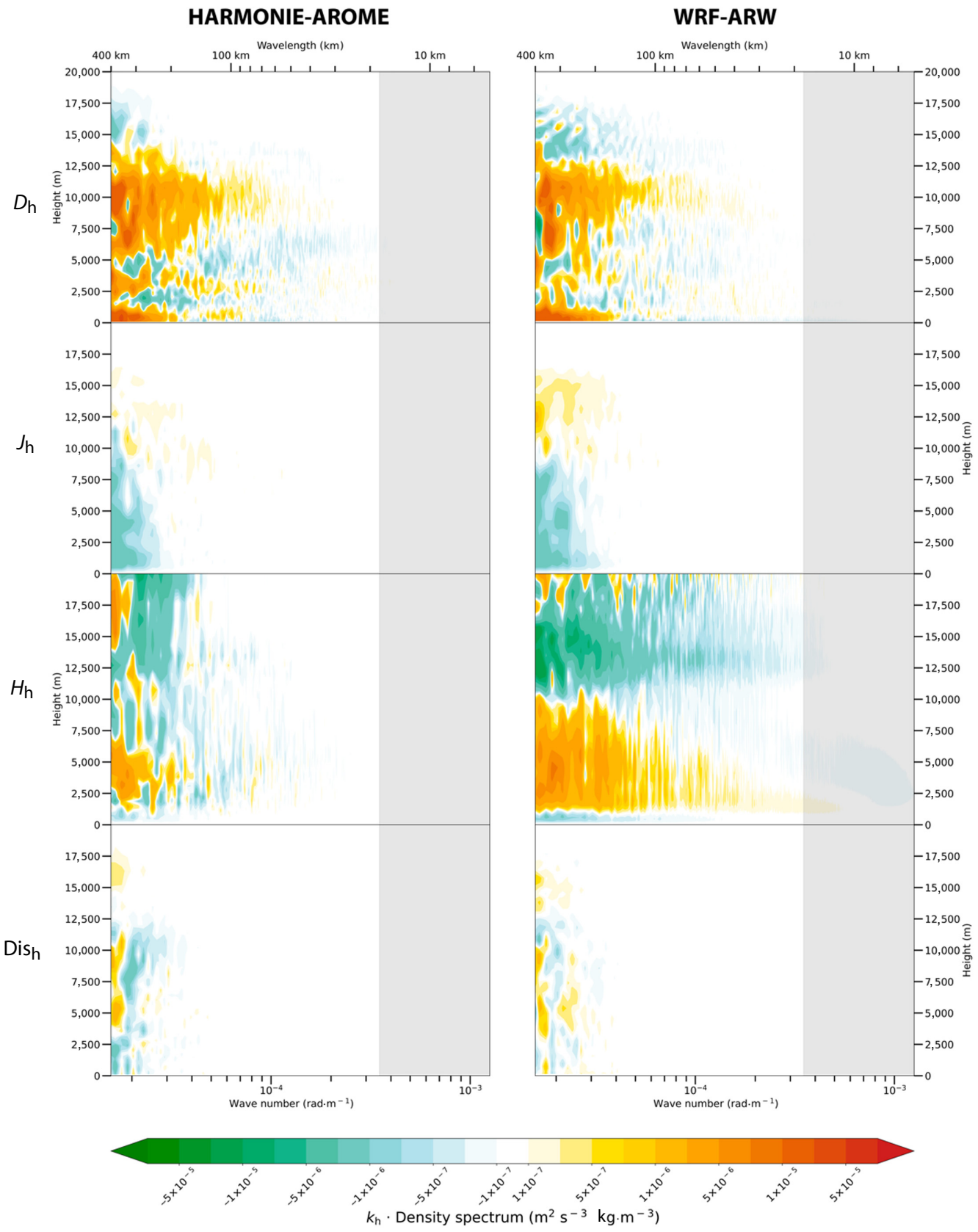

FIGURE 8 As Figure 7 except for mesoscale for the HARMONIE-AROME and Weather Research and Forecasting (WRF) simulations. ARW: Advanced Research WRF. Note that the limits of the colour bar are different from Figure 7. [Colour figure can be viewed at wileyonlinelibrary.com]

et al., 2022). In the mesoscale range (Figure 8), $\mathrm{Dis_h}$ is almost non-existent for $\lambda_h < 200$ km. These results are in contradiction with Hamilton *et al.* (2008), who finds that the dissipation affects mainly the smaller wavelengths, being negligible for most of the mesoscale. However, Wang *et al.* (2018) find notable values in the synoptic scale and mesoscale, with a negative peak at $\lambda_h \approx 500$ km. The vertical averages of $\mathrm{Dis_h}$ (Supporting Information Figures S3 and S4) depict a null contribution to the HKE spectrum.

Evaluating the energetic behaviour of TT *Delta* as a whole, the forcing of HKE is governed by t_h, D_h, and H_h. The terms $C_{A\to h}$, $\partial_z F_{p\uparrow}$, and $\partial_z F_{h\uparrow}$ are secondary contributors, whereas J_h and $\mathrm{Dis_h}$ are only minor variables. There is evidence to state that the HKE spectrum in this case study is greatly affected by the latent heating associated with the moist processes of the TT, supporting energy propagation. These promote positive contributions to the mesoscale APE while enhancing the vertical convection by the conversion of APE to HKE. The results also show that the major energetic contributions (positive and negative) come from the synoptic range. According to Peng *et al.* (2015b), the net direct forcing of the spectral budget, defined as the summation of all the terms of Equation (2) except t_h and $\mathrm{Dis_h}$, reveals how the troposphere is energized at different scales. In this case, the net direct forcing (Supporting Information Figure S5) at the synoptic scale shows a transfer of energy from the low and middle levels to the upper troposphere for $\lambda_h > 1{,}000$ km. In the range $1{,}000 < \lambda_h < 800$ km all the levels present a negative forcing in favour of the stratosphere (most clearly shown in WRF). For $\lambda_h < 800$ km, there is a weak positive forcing for all the troposphere, propagating into the mesoscale. In the mesoscale, the near surface and the high troposphere show a negative net forcing, with positive values for the midlevels, which reveals that most of the energy is taken from lower and upper levels and transferred to the midtroposphere. The thickness of this midtroposphere band presents large differences between the models, being much wider and constant for WRF, but being irregular and thin for HAR.

The final piece of this discussion is the change of behaviour of the different terms between the synoptic scale and the mesoscale. Though the results for the mesoscale seem to be dependent on the vertical levels (horizontal bands with similar characteristics across the wavelength range in Figures 5 and 8), the energy behaviour for the synoptic scale is much more complex and seems to be dependant mostly on the wavelength (vertical bands across the levels in Figures 4 and 7). This might be related to the irruption of an overenergetic event like a TT precisely at the lower synoptic wavelengths range, in the typical TT extension ($1{,}000 > \lambda_h > 400$ km). The strong vertical forcing induced by the many effects associated with TTs seems to produce a very complex and heterogeneous energy system, where the relationship between the different terms is not completely clear and the transfer and conversion of energy is very hard to track. Clearly, the HKE spectrum is not sufficient to explain the energetic behaviour of TTs, and even the energy budget requires more research.

4 | SUMMARY AND CONCLUSIONS

This work evaluates the energy spectral behaviour of the simulation of TTs in the North Atlantic area, following previous studies by Peng, Zhang, Luo, and Zhang (2014), Sun *et al.* (2017), Wang *et al.* (2018), and Zheng *et al.* (2020), based on the methodology by Skamarock (2004), Denis *et al.* (2002), Peng *et al.* (2015a, 2015b), and Sun *et al.* (2017), and in continuation of previous studies by Bolgiani *et al.*, (2020; 2022). The aim of this study is to assess the HKE spectra and spectral budgets to evaluate the accuracy of the WRF and HARMONIE-AROME models in TTs simulations. The simulations are generated using the WRF and HAR models, at 2.5 km grid resolution, taking the ERA5 as initial/boundary conditions. The HKE spectra of four highly energetic TT events are first assessed for the 500 hPa, and the energy budget of the TT *Delta* is then evaluated. The major conclusions are as follows:

- The WRF model results show how the energy is assumed from the initial/boundary conditions and computed into realistic energy spectra with smaller grid resolutions, properly capturing the $k^{-5/3}$ transition when the resolution is adequate.
- The four TTs evaluated present notable differences among the HKE spectra, probably related to the wind-speed intensities. Nevertheless, all of them show a highly energetic state at synoptic scales.
- Globally, both models present similar spectra. However, WRF results are consistently more energetic than HAR, especially at the smaller wavelengths, denoting a steeper numerical dissipation by HAR.
- The results of the spectral budget for TT *Delta* are also similar for both models, and the differences are mainly located in the stratosphere, most probably due to the differences in vertical resolution.
- The HKE spectral budget is mainly governed by t_h, D_h, and H_h, mainly above $\lambda_h > 1{,}000$ km. Whereas D_h and H_h present positive contributions, t_h is negative for $\lambda_h < 2{,}000$ km, but presents a large positive pool for $\lambda_h > 2{,}000$ km. The combined contributions partially explain the overenergetic spectrum. This is also assisted by the synoptic flow of t_h inhibiting the direct cascade at tropical-storm-size wavelengths.

- The contributions of $C_{A\to h}$, $\partial_z F_{p\uparrow}$, and $\partial_z F_{h\uparrow}$ are relatively moderate. However, these terms greatly affect the spectrum at the synoptic scale and mesoscale, highlighting that the roles of moist convection and latent heat can exceed the energy cascade and other energy transfer processes. $F_{h\uparrow}$ is predominant at the synoptic scale and $F_{p\uparrow}$ is predominant at the mesoscale.
- At the mesoscale, the contribution of each term seems to be dependent on the vertical levels. However, at synoptic scales the terms have a much more complex behaviour, which seems to be dependent on the wavelengths.

Overall, it is clear that a high-energetic system, such as a TT, can notably affect the atmospheric energy spectrum. The energy budget of TT events shows a very complex behaviour far from the simple energy cascade theory, presenting a three-dimensional transfer and contribution of energy, in line with the results of the Sun *et al.* (2017), Wang *et al.* (2018), and Zheng *et al.* (2020). Moreover, the energy transfer is very dependent on the strong links existing between vertical levels. Both, WRF and HAR models are coincident in most of the results; however, more research is required to fully grasp the energetic configuration of TTs and how each process affects the building of the HKE spectrum.

AUTHOR CONTRIBUTIONS

Carlos Calvo-Sancho: Data curation; formal analysis; investigation; methodology; resources; software; validation; visualization; writing – original draft; writing – review and editing. **Pedro Bolgiani:** Conceptualization; data curation; formal analysis; methodology; resources; visualization; writing – original draft; writing – review and editing. **Álvaro Subias:** Data curation; formal analysis; investigation; methodology; resources; software; validation; writing – original draft; writing – review and editing. **Mariano Sastre:** Formal analysis; investigation; methodology; resources; supervision; writing – original draft; writing – review and editing. **Juan Jesús González-Alemán:** Formal analysis; investigation; methodology; writing – original draft; writing – review and editing. **María Luisa Martín:** Conceptualization; data curation; formal analysis; funding acquisition; investigation; methodology; project administration; resources; supervision; validation; visualization; writing – original draft; writing – review and editing.

ACKNOWLEDGEMENTS

This work was partially supported by research project PID2019-105306RB-I00/AEI/10.13039/501100011033 (IBERCANES). This work is supported by the Interdisciplinary Mathematics Institute of the Complutense University of Madrid. This work is also supported by the ECMWF Special Projects SPESMART and SPESVALE. C. Calvo-Sancho acknowledges the grant awarded by the Spanish Ministry of Science and Innovation–FPI program (PRE2020-092343).

FUNDING INFORMATION

This work is funded by the Spanish Ministry of Economy under the research project PID2019-105306RB-I00/AEI/10.13039/501100011033 (IBERCANES). This work is also supported by the ECMWF Special Projects SPESMART and SPESVALE.

CONFLICT OF INTEREST

The authors declare no conflict of interest. The funding sponsors have no participation in the execution of the experiment, the decision to publish the results, nor the writing of the manuscript.

ORCID

Carlos Calvo-Sancho https://orcid.org/0000-0003-2457-9793
Pedro Bolgiani https://orcid.org/0000-0002-7096-5831
Álvaro Subias https://orcid.org/0000-0003-4457-835X
Mariano Sastre https://orcid.org/0000-0002-5757-3956
Juan Jesús González-Alemán https://orcid.org/0000-0001-5940-7356
María Luisa Martín https://orcid.org/0000-0002-8500-8276

REFERENCES

Abdalla, S., Isaksen, L., Janssen, P. and Wedi, N. (2013) Effective spectral resolution of ECMWF atmospheric forecast models. *ECMWF Newsletter*, 137, 19–22. https://doi.org/10.21957/RUE4O7AC.

Augier, P. and Lindborg, E. (2013) A new formulation of the spectral energy budget of the atmosphere, with application to two high-resolution general circulation models. *Journal of the Atmospheric Sciences*, 70, 2293–2308. https://doi.org/10.1175/JAS-D-12-0281.1.

Bannon, P.R. (2005) Eulerian available energetics in moist atmospheres. *Journal of the Atmospheric Sciences*, 62(12), 4238–4252.

Becker, E. (2001) Symmetric stress tensor formulation of horizontal momentum diffusion in global models of atmospheric circulation. *Journal of the Atmospheric Sciences*, 58(3), 269–282.

Bengtsson, L., Andrae, U., Aspelien, T., Batrak, Y., Calvo, J., de Rooy, W., Gleeson, E., Hansen-Sass, B., Homleid, M., Hortal, M. and Ivarsson, K.I. (2017) The HARMONIE–AROME model configuration in the ALADIN–HIRLAM NWP system. *Monthly Weather Review*, 145(5), 1919–1935.

Bentley, A.M., Bosart, L.F. and Keyser, D. (2017) Upper-tropospheric precursors to the formation of subtropical cyclones that

undergo tropical transition in the North Atlantic basin. *Monthly Weather Review*, 145, 503–520. https://doi.org/10.1175/MWR-D-16-0263.1.

Beven, J.L., Beven, J.L., Avila, L.A., Blake, E.S., Brown, D.P., Franklin, J.L., Knabb, R.D., Pasch, R.J., Rhome, J.R. and Stewart, S.R. (2008) Atlantic hurricane season of 2005. *Monthly Weather Review*, 139, 1109–1173.

Bierdel, L., Friederichs, P. and Bentzien, S. (2012) Spatial kinetic energy spectra in the convection-permitting limited-area NWP model COSMO-DE. *Meteorologische Zeitschrift*, 21, 245–258. https://doi.org/10.1127/0941-2948/2012/0319.

Bolgiani, P., Calvo-Sancho, C., Díaz-Fernández, J., Quitián-Hernández, L., Sastre, M., Santos-Muñoz, D., Farrán, J.I., González-Alemán, J.J., Valero, F. and Martín, M.L. (2022) Wind kinetic energy climatology and effective resolution for the ERA5 reanalysis. *Climate Dynamics*, 59, 737–752. https://doi.org/10.1007/s00382-022-06154-y.

Bolgiani, P., Santos-Muñoz, D., Fernández-González, S., Sastre, M., Valero, F. and Martín, M.L. (2020) Microburst detection with the WRF model: effective resolution and forecasting indices. *JGR-Atmospheres*, 125, e2020JD032883. https://doi.org/10.1029/2020JD032883.

Boville, B.A. and Bretherton, C.S. (2003) Heating and kinetic energy dissipation in the NCAR community atmosphere model. *Journal of Climate*, 16, 3877–3887. https://doi.org/10.1175/1520-0442(2003)016<3877:HAKEDI>2.0.CO;2.

Bracken, W.E. and Bosart, L.F. (2000) The role of synoptic-scale flow during tropical cyclogenesis over the North Atlantic Ocean. *Monthly Weather Review*, 128(2), 353–376.

Calvo-Sancho, C., González-Alemán, J.J., Bolgiani, P., Santos-Muñoz, D., Farrán, J.I. and Martín, M.L. (2022) An environmental synoptic analysis of tropical transitions in the central and eastern North Atlantic. *Atmospheric Research*, 278, 106353. https://doi.org/10.1016/j.atmosres.2022.106353.

Cho, J.Y.N., Newell, R. and Barrick, J.D. (1999) Horizontal wavenumber spectra of winds, temperature, and trace gases during the Pacific Exploratory Missions: 1. Climatology. *Journal of Geophysical Research-Atmospheres*, 104, 5697–5716.

Davis, C.A. and Bosart, L.F. (2003) Baroclinically induced tropical cyclogenesis. *Monthly Weather Review*, 131, 2730–2747. https://doi.org/10.1175/1520-0493(2003)131<2730:BITC>2.0.CO;2.

Davis, C.A. and Bosart, L.F. (2004) The TT problem: forecasting the tropical transition of cyclones. *Bulletin of the American Meteorological Society*, 85(11), 1657–1662. https://doi.org/10.1175/BAMS-85-11-1657.

DeMaria, M., Knaff, J.A. and Connell, B.H. (2001) A tropical cyclone genesis parameter for the tropical Atlantic. *Weather and Forecasting*, 16, 219–233. https://doi.org/10.1175/1520-0434(2001)016<0219:ATCGPF>2.0.CO;2.

Denis, B., Côté, J. and Laprise, R. (2002) Spectral decomposition of two-dimensional atmospheric fields on limited-area domains using the discrete cosine transform (DCT). *Monthly Weather Review*, 130, 1812–1829. https://doi.org/10.1175/1520-0493(2002)130<1812:SDOTDA>2.0.CO;2.

Díaz-Fernández, J., Bolgiani, P., Santos-Muñoz, D., Quitián-Hernández, L., Sastre, M., Valero, F., Gonzalez-Aleman, J.J. and Martín, M.L. (2022) Comparison of the WRF and HARMONIE models ability for mountain wave warnings. *Atmospheric Research*, 265, 105890. https://doi.org/10.1016/j.atmosres.2021.105890.

Díaz-Fernández, J., Bolgiani, P., Sastre, M., Santos-Muñoz, D., Valero, F., Farran, J.I. and Martin, M.L. (2022) Ability of the WRF-ARW and HARMONIE-AROME models to detect turbulence related to mountain waves over Central Iberia. *Atmospheric Research*, 274, 106183. https://doi.org/10.1016/j.atmosres.2022.106183.

Dudhia, J. (1989) Numerical study of convection observed during the winter monsoon experiment using a mesoscale two-dimensional model. *Journal of Atmospheric Sciences*, 46(20), 3077–3107.

Durran, D.R. and Weyn, J.A. (2016) Thunderstorms do not get butterflies. *Bulletin of the American Meteorological Society*, 97(2), 237–243.

Ferreira, R.N. and Schubert, W.H. (1999). The role of tropical cyclones in the formation of tropical upper-tropospheric troughs. *Journal of the Atmospheric Sciences*, 56(16), 2891–2907.

Gage, K.S. (1979) Evidence far a k- 5/3 law inertial range in mesoscale two-dimensional turbulence. *Journal of Atmospheric Sciences*, 36(10), 1950–1954.

Galarneau, T.J., McTaggart-Cowan, R., Bosart, L.F. and Davis, C.A. (2015) Development of North Atlantic tropical disturbances near upper-level potential vorticity streamers. *Journal of the Atmospheric Sciences*, 72, 572–597. https://doi.org/10.1175/JAS-D-14-0106.1.

Gray, W.M. (1968) Global view of the origin of tropical disturbances and storms. *Monthly Weather Review*, 96, 669–700. https://doi.org/10.1175/1520-0493(1968)096%3C0669:GVOTOO%3E2.0.CO;2.

Hamilton, K., Takahashi, Y.O. and Ohfuchi, W. (2008) Mesoscale spectrum of atmospheric motions investigated in a very fine resolution global general circulation model. *Journal of Geophysical Research*, 113, D18110. https://doi.org/10.1029/2008JD009785.

Hersbach, H., Bell, B., Berrisford, P., Hirahara, S., Horányi, A., Muñoz-Sabater, J., Nicolas, J., Peubey, C., Radu, R., Schepers, D., Simmons, A., Soci, C., Abdalla, S., Abellan, X., Balsamo, G., Bechtold, P., Biavati, G., Bidlot, J., Bonavita, M., et al. (2020) The ERA5 global reanalysis. *Quarterly Journal of the Royal Meteorological Society*, 146(730), 1999–2049. https://doi.org/10.1002/qj.3803.

Holtslag, A.A.M. and Boville, B.A. (1993) Local versus nonlocal boundary-layer diffusion in a global climate model. *Journal of climate*, 6(10), 1825–1842.

Hong, S.Y. and Lim, J.O.J. (2006) The WRF single-moment 6-class microphysics scheme (WSM6). *Asia-Pacific Journal of Atmospheric Sciences*, 42(2), 129–151.

Hong, S.Y., Noh, Y. and Dudhia, J. (2006) A new vertical diffusion package with an explicit treatment of entrainment processes. *Monthly Weather Review*, 134(9), 2318–2341.

Hulme, A.L. and Martin, J.E. (2009) Synoptic- and frontal-scale influences on tropical transition events in the Atlantic Basin. Part I: a six-case survey. *Monthly Weather Review*, 137, 3605–3625. https://doi.org/10.1175/2009MWR2802.1.

Hutchinson, T.A. (2007) An adaptive time-step for increased model efficiency. In Extended Abstracts, Eighth WRF Users' Workshop (p. 4).

Kolmogorov, A.N. (1941) The local structure of turbulence in incompressible viscous fluid for very large Reynolds numbers. *Doklady Akademii Nauk*, 30, 9–13. https://doi.org/10.1098/rspa.1991.0075.

Koshyk, J.N. and Hamilton, K. (2001) The horizontal kinetic energy spectrum and spectral budget simulated by a high-resolution troposphere-stratosphere-mesosphere GCM. *Journal of the Atmospheric Sciences*, 58(4), 329–348. https://doi.org/10.1175/1520-0469(2001)058<0329:THKESA>2.0.CO;2.

Landsea, C.W. and Franklin, J.L. (2013) Atlantic hurricane database uncertainty and presentation of a new database format. *Monthly Weather Review*, 141(10), 3576–3592.

Lascaux, F., Richard, E. and Pinty, J.P. (2006) Numerical simulations of three different MAP IOPs and the associated microphysical processes. *Quarterly Journal of the Royal Meteorological Society: A Journal of the Atmospheric Sciences, Applied Meteorology and Physical Oceanography*, 132(619), 1907–1926.

Lenzen, M., Malik, A., Kenway, S., Daniels, P., Lam, K.L. and Geschke, A. (2019) Economic damage and spillovers from a tropical cyclone. *Natural Hazards and Earth System Sciences*, 19, 137–151. https://doi.org/10.5194/nhess-19-137-2019.

Lindborg, E. (1999) Can the atmospheric kinetic energy spectrum be explained by two-dimensional turbulence? *Journal of Fluid Mechanics*, 388, 259–288. https://doi.org/10.1017/S0022112099004851.

Lindborg, E. (2005) The effect of rotation on the mesoscale energy cascade in the free atmosphere. *Geophysical Research Letters*, 32, L01809, https://doi.org/10.1029/2004GL021319.

Lorenz, E.N. (1969) The predictability of a flow which possesses many scales of motion. *Tellus*, 21, 289–307. https://doi.org/10.1111/j.2153-3490.1969.tb00444.x.

Martius, O., Schwierz, C. and Sprenger, M. (2008) Dynamical tropopause variability and potential vorticity streamers in the Northern hemisphere—a climatological analysis. *Advances in Atmospheric Sciences*, 25, 367–380. https://doi.org/10.1007/s00376-008-0367-z.

McIntyre, M.E. and Palmer, T.N. (1983) Breaking planetary waves in the stratosphere. *Nature*, 305, 593–600. https://doi.org/10.1038/305593a0.

McTaggart-Cowan, R., Davies, E.L., Fairman, J.G., Galarneau, T.J. and Schultz, D.M. (2015) Revisiting the 26.5°C sea surface temperature threshold for tropical cyclone development. *Bulletin of the American Meteorological Society*, 96, 1929–1943. https://doi.org/10.1175/BAMS-D-13-00254.1.

McTaggart-Cowan, R., Deane, G.D., Bosart, L.F., Davis, C.A. and Galarneau, T.J. (2008) Climatology of tropical cyclogenesis in the North Atlantic (1948–2004). *Monthly Weather Review*, 136, 1284–1304. https://doi.org/10.1175/2007MWR2245.1.

McTaggart-Cowan, R., Galarneau, T.J., Bosart, L.F., Moore, R.W. and Martius, O. (2013) A global climatology of baroclinically influenced tropical cyclogenesis. *Monthly Weather Review*, 141, 1963–1989. https://doi.org/10.1175/MWR-D-12-00186.1.

Mlawer, E.J., Taubman, S.J., Brown, P.D., Iacono, M.J. and Clough, S.A. (1997) Radiative transfer for inhomogeneous atmospheres: RRTM, a validated correlated-k model for the longwave. *Journal of Geophysical Research-Atmospheres*, 102(D14), 16663–16682.

Moore, P. (2021) An analysis of storm Ophelia which struck Ireland on 16 October 2017. *Weather*, 76(9), 301–306.

Molinari, J., Vollaro, D. and Corbosiero, K.L. (2004) Tropical cyclone formation in a sheared environment: A case study. *Journal of the Atmospheric Sciences*, 61(21), 2493–2509.

Nastrom, G.D. and Gage, K.S. (1985) A climatology of atmospheric wavenumber spectra of wind and temperature observed by commercial aircraft. *Journal of the Atmospheric Sciences*, 42(9), 950–960. https://doi.org/10.1175/1520-0469(1986)043<0729:TIOAWS>2.0.CO;2.

Nieto, R., Gimeno, L., de la Torre, L., Ribera, P., Gallego, D., García-Herrera, R., García, J.A., Nuñez, M., Redaño, A. and Lorente, J. (2005) Climatological features of cutoff low systems in the Northern Hemisphere. *Journal of Climate*, 18, 3085–3103. https://doi.org/10.1175/JCLI3386.1.

Nyquist, H. (1928) Certain topics in telegraph transmission theory. *Transactions of the American Institute of Electrical Engineers*, 47(2), 617–644. https://doi.org/10.1109/T-AIEE.1928.5055024.

Palmén, E. and Newton, C.W. (1969) Atmospheric circulation systems: their structural and physical interpretation. *Science*, 167, 972.

Patla, J.E., Stevens, D. and Barnes, G.M. (2009) A conceptual model for the influence of TUTT cells on tropical cyclone motion in the Northwest Pacific Ocean. *Weather and Forecasting*, 24, 1215–1235.

Pauluis, O. and Held, I.M. (2002) Entropy budget of an atmosphere in radiative–convective equilibrium. Part II: latent heat transport and moist processes. *Journal of the Atmospheric Sciences*, 59(2), 140–149.

Peduzzi, P., Chatenoux, B., Dao, H., De Bono, A., Herold, C., Kossin, J., Mouton, F. and Nordbeck, O. (2012) Global trends in tropical cyclone risk. *Nature Climate Change*, 2, 289–294. https://doi.org/10.1038/nclimate1410.

Peng, J., Zhang, L. and Guan, J. (2015a) Applications of a moist nonhydrostatic formulation of the spectral energy budget to baroclinic waves. Part I: the lower-stratospheric energy spectra. *Journal of the Atmospheric Sciences*, 72, 2090–2108. https://doi.org/10.1175/JAS-D-14-0306.1.

Peng, J., Zhang, L. and Guan, J. (2015b) Applications of a moist nonhydrostatic formulation of the spectral energy budget to baroclinic waves. Part II: the upper-tropospheric energy spectra. *Journal of the Atmospheric Sciences*, 72, 3923–3939. https://doi.org/10.1175/JAS-D-14-0359.1.

Peng, J., Zhang, L., Luo, Y. and Xiong, C. (2014a) Mesoscale energy spectra of the Mei-Yu front system. Part II: moist available potential energy spectra. *Journal of the Atmospheric Sciences*, 71, 1410–1424. https://doi.org/10.1175/JAS-D-13-0319.1.

Peng, J., Zhang, L., Luo, Y. and Zhang, Y. (2014b) Mesoscale energy spectra of the Mei-Yu front system. Part I: kinetic energy spectra. *Journal of the Atmospheric Sciences*, 71, 37–55. https://doi.org/10.1175/JAS-D-13-085.1.

Quitián-Hernández, L., Bolgiani, P., Santos-Muñoz, D., Sastre, M., Díaz-Fernández, J., González-Alemán, J.J., Farrán, J.I., Lopez, L., Valero, F. and Martín, M.L. (2021) Analysis of the October 2014 subtropical cyclone using the WRF and the HARMONIE-AROME numerical models: assessment against observations. *Atmospheric Research*, 260, 105697.

Rai, R.K., Berg, L.K., Kosović, B., Mirocha, J.D., Pekour, M.S. and Shaw, W.J. (2017) Comparison of measured and numerically simulated turbulence statistics in a convective boundary layer over complex terrain. *Boundary-Layer Meteorology*, 163, 69–89.

Ricard, D., Lac, C., Riette, S., Legrand, R. and Mary, A. (2013) Kinetic energy spectra characteristics of two convection-permitting limited-area models AROME and Meso-NH: KE spectra characteristics of two convection-permitting models. *Quarterly Journal*

of the Royal Meteorological Society, 139, 1327–1341. https://doi.org/10.1002/qj.2025.

Román-Cascón, C., Yagüe, C., Steeneveld, G.J., Morales, G., Arrillaga, J.A., Sastre, M. and Maqueda, G. (2019) Radiation and cloud-base lowering fog events: observational analysis and evaluation of WRF and HARMONIE. *Atmospheric Research*, 229, 190–207. https://doi.org/10.1016/j.atmosres.2019.06.018.

de Rooy, W.C., Bechtold, P., Fröhlich, K., Hohenegger, C., Jonker, H., Mironov, D., Pier Siebesma, A., Teixeira, J. and Yano, J.I. (2013) Entrainment and detrainment in cumulus convection: An overview. *Quarterly Journal of the Royal Meteorological Society*, 139(670), 1–19.

Sadler, J. C. (1976). A role of the tropical upper tropospheric trough in early season typhoon development. *Monthly Weather Review*, 104(10), 1266–1278.

Sanchez-Laulhe, J.M. and Martin, F. (2006) Analysis of the extratropical transition of the tropical cyclone Delta. 5a Asamblea Hispano-Portuguesa de Geodesia y Geofisica, 4 pp. ISBN: 84-8320-373-1.

Seco, A., González, P.J., Ramírez, F., García, R., Prieto, E., Yagüe, C. and Fernández, J. (2009) GPS monitoring of the tropical storm delta along the Canary Islands track, November 28-29, 2005. *Pure and Applied Geophysics*, 166, 1519–1531.

Seity, Y., Brousseau, P., Malardel, S., Hello, G., Bénard, P., Bouttier, F., Lac, C. and Masson, V. (2011) The AROME-France convective-scale operational model. *Monthly Weather Review*, 139(3), 976–991.

Selz, T. and Craig, G.C. (2015) Simulation of upscale error growth with a stochastic convection scheme. *Geophysical Research Letters*, 42(8), 3056–3062.

Skamarock, W.C. (2004) Evaluating mesoscale NWP models using kinetic energy spectra. *Monthly Weather Review*, 132, 3019–3032. https://doi.org/10.1175/MWR2830.1.

Skamarock, W.C., Klemp, J.B., Dudhia, J., Gill, D.O., Barker, D.M., Wang, W. and Powers, J.G. (2008) A description of the Advanced Research WRF version 3. NCAR Technical note-475+STR.

Skamarock, W.C., Park, S.-H., Klemp, J.B. and Snyder, C. (2014) Atmospheric kinetic energy spectra from global high-resolution nonhydrostatic simulations. *Journal of the Atmospheric Sciences*, 71, 4369–4381. https://doi.org/10.1175/JAS-D-14-0114.1.

Sun, Y.Q., Rotunno, R. and Zhang, F. (2017) Contributions of moist convection and internal gravity waves to building the atmospheric −5/3 kinetic energy spectra. *Journal of the Atmospheric Sciences*, 74, 185–201. https://doi.org/10.1175/JAS-D-16-0097.1.

Sun, Y.Q. and Zhang, F. (2016) Intrinsic versus practical limits of atmospheric predictability and the significance of the butterfly effect. *Journal of the Atmospheric Sciences*, 73(3), 1419–1438.

Tapiador, F.J., Gaertner, M.A., Romera, R. and Castro, M. (2007) A multisource analysis of Hurricane Vince. *Bulletin of the American Meteorological Society*, 88, 1027–1032. https://doi.org/10.1175/BAMS-88-7-1027.

Thorncroft, C.D., Hoskins, B.J. and McIntyre, M.E. (1993) Two paradigms of baroclinic-wave life-cycle behaviour. *Quarterly Journal of the Royal Meteorological Society*, 119, 17–55. https://doi.org/10.1002/qj.49711950903.

Tulloch, R. and Smith, K.S. (2006) A theory for the atmospheric energy spectrum: depth-limited temperature anomalies at the tropopause. *Proceedings of the National Academy of Sciences of the United States of America*, 103(40), 14690–14694. https://doi.org/10.1073/pnas.0605494103.

Tung, K.K. and Orlando, W.W. (2003) On the difference between 2D and QG turbulence. *Discrete and Continuous Dynamical Systems*, 3(2), 145–162.

Vonich, P.T. and Hakim, G.J. (2018) Hurricane kinetic energy spectra from in situ aircraft observations. *Journal of the Atmospheric Sciences*, 75, 2523–2532. https://doi.org/10.1175/JAS-D-17-0270.1.

Waite, M.L. and Snyder, C. (2013) Mesoscale energy spectra of moist baroclinic waves. *Journal of the Atmospheric Sciences*, 70, 1242–1256. https://doi.org/10.1175/JAS-D-11-0347.1.

Wang, Y., Zhang, L., Peng, J. and Liu, S. (2018) Mesoscale horizontal kinetic energy spectra of a tropical cyclone. *Journal of the Atmospheric Sciences*, 75, 3579–3596. https://doi.org/10.1175/JAS-D-17-0391.1.

Weyn, J.A. and Durran, D.R. (2017) The dependence of the predictability of mesoscale convective systems on the horizontal scale and amplitude of initial errors in idealized simulations. *Journal of the Atmospheric Sciences*, 74(7), 2191–2210.

Williamson, D.L. (2002) Time-split versus process-split coupling of parameterizations and dynamical core. *Monthly Weather Review*, 130(8), 2024–2041.

Zhang, C. and Wang, Y. (2017) Projected future changes of tropical cyclone activity over the western North and South Pacific in a 20-km-mesh regional climate model. *Journal of Climate*, 30(15), 5923–5941.

Zheng, H., Zhang, Y., Wang, Y., Zhang, L., Peng, J., Liu, S. and Li, A. (2020) Characteristics of atmospheric kinetic energy spectra during the intensification of Typhoon Lekima (2019). *Applied Sciences*, 10, 6029. https://doi.org/10.3390/app10176029.

SUPPORTING INFORMATION

Additional supporting information can be found online in the Supporting Information section at the end of this article.

How to cite this article: Calvo-Sancho, C., Bolgiani, P., Subias, Á., Sastre, M., González-Alemán, J.J. & Martín, M.L. (2023) Horizontal kinetic energy analysis of tropical transition simulations with the WRF and HARMONIE-AROME models. *Quarterly Journal of the Royal Meteorological Society*, 149(756), 2655–2677. Available from: https://doi.org/10.1002/qj.4523